Efferocytosis of SARS-CoV-2-infected dying cells impairs macrophage anti-inflammatory functions and clearance of apoptotic cells

Ana C. G. Salina[1†], Douglas dos-Santos[1†], Tamara S. Rodrigues[1†], Marlon Fortes-Rocha[1], Edismauro G. Freitas-Filho[1], Daniel L. Alzamora-Terrel[1], Ícaro M. S. Castro[2], Thais F. C. Fraga da Silva[3], Mikhael H. F. de Lima[4], Daniele C. Nascimento[4], Camila M. Silva[4], Juliana E. Toller-Kawahisa[4], Amanda Becerra[1], Samuel Oliveira[1], Diego B. Caetité[4], Leticia Almeida[1,5], Adriene Y. Ishimoto[1], Thais M. Lima[1], Ronaldo B. Martins[1], Flavio Veras[4,5], Natália B. do Amaral[6], Marcela C. Giannini[6], Letícia P. Bonjorno[6], Maria I. F. Lopes[6], Maira N. Benatti[8], Sabrina S. Batah[8], Rodrigo C. Santana[6], Fernando C. Vilar[6], Maria A. Martins[7], Rodrigo L. Assad[6], Sergio C. L. de Almeida[6], Fabiola R. de Oliveira[6], Eurico Arruda Neto[1], Thiago M. Cunha[4,5], José C. Alves-Filho[4,5], Vânia L. D. Bonato[3], Fernando Q. Cunha[4,5], Alexandre T. Fabro[8], Helder I. Nakaya[2,5], Dario S. Zamboni[1,5], Paulo Louzada-Junior[5,6], Rene D. R. Oliveira[6], Larissa D. Cunha[1]*

[1]Departamento de Biologia Celular e Molecular e Bioagentes Patogênicos, Faculdade de Medicina de Ribeirão Preto, Universidade de São Paulo, Ribeirão Preto, SP, Brazil.
[2]Departamento de Análises Clínicas e Toxicológicas, Faculdade de Ciências Farmacêuticas, Universidade de São Paulo, Brazil.
[3]Departamento de Bioquímica e Imunologia, Faculdade de Medicina de Ribeirão Preto, Universidade de São Paulo, Ribeirão Preto, São Paulo, Brazil.
[4]Departamento de Farmacologia, Faculdade de Medicina de Ribeirão Preto, Universidade de São Paulo, Ribeirão Preto, São Paulo, Brazil.
[5]Center of Research in Inflammatory Diseases (CRID), Faculdade de Medicina de Ribeirão Preto, Universidade de São Paulo, Ribeirão Preto, São Paulo, Brazil.
[6]Divisão de Imunologia Clinica, Emergência, Doenças Infecciosas e Unidade de Terapia Intensiva, Faculdade de Medicina de Ribeirão Preto, Universidade de São Paulo, Ribeirão Preto, SP, Brazil.
[7]Departamento de Cirurgia e Anatomia, Faculdade de Medicina de Ribeirão Preto, Universidade de São Paulo, Ribeirão Preto, SP, Brazil.
[8]Departamento de Patologia e Medicina Legal, Faculdade de Medicina de Ribeirão Preto, Universidade de São Paulo, Ribeirão Preto, SP, Brazil.

† A.C.G.S., D.S., and T.S.R. equally contributed to this work.

* Correspondence: Departamento de Biologia Celular e Molecular e Bioagentes Patogênicos
Faculdade de Medicina de Ribeirão Preto, Universidade de São Paulo
Av. Bandeirantes 3900, Ribeirão Preto, SP 14049-900, Brazil
Tel: +55 16 33153319
larissacunha@usp.br
(ORCID iD: 0000-0002-1290-0263),

Abstract

COVID-19 is a disease of dysfunctional immune responses, but the mechanisms triggering immunopathogenesis are not established. The functional plasticity of macrophages allows this cell type to promote pathogen elimination and inflammation or suppress inflammation and promote tissue remodeling and injury repair. During an infection, the clearance of dead and dying cells, a process named efferocytosis, can modulate the interplay between these contrasting functions. Here, we show that engulfment of SARS-CoV2-infected apoptotic cells exacerbates inflammatory cytokine production, inhibits the expression of efferocytic receptors, and impairs continual efferocytosis by macrophages. We also provide evidence supporting that lung monocytes and macrophages from severe COVID-19 patients have compromised efferocytic capacity. Our findings reveal that dysfunctional efferocytosis of SARS-CoV-2-infected cell corpses suppress macrophage anti-inflammation and efficient tissue repair programs and provide mechanistic insights for the excessive production of pro-inflammatory cytokines and accumulation of tissue damage associated with COVID-19 immunopathogenesis.

KEYWORDS: COVID-19, macrophage, macrophage polarization, efferocytosis, hyperinflammation, tissue repair

Introduction

Patients with severe and critical COVI-19 progress from pneumonia to development of acute respiratory distress syndrome (ARDS) and respiratory failure, septic shock, and multiorgan dysfunction (Siddiqi and Mehra, 2020). These severe clinical manifestations of the disease are caused by dysregulated host immune response, including compromised function of the myeloid compartment (Blanco-Melo et al., 2020; Lucas et al., 2020; Rodrigues et al., 2020; Schulte-Schrepping et al., 2020; Silvin et al., 2020; Valle et al., 2020; Veras et al., 2020). Therefore, hyperinflammation and extensive unresolved tissue damage associated with dysfunctional innate responses should contribute to the pathogenesis of inflammatory lung disease and worsening of COVID-19, although underlying mechanisms are still loosely defined.

Macrophages and monocytes are functionally plastic cells that can promote homeostasis and resolution of inflammation by sensing microbial and host-derived signals and programming their gene expression toward an anti-inflammatory, pro-resolution, and wound-healing phenotype (Martins et al., 2019; (Trzebanski and Jung, 2020). This host-protective programming reduces inflammatory cytokine production by other immune and non-immune cells and promotes the repair of damaged tissue to sustain physiological function and re-establish homeostasis (Murray and Wynn, 2011). During the repair process, the efficient clearance of dying cells prevents further tissue dysfunction caused by uncontrolled cytotoxicity and the release of damage-associated molecular patterns (DAMP). Defects in sensing, ingesting, and degradation of dead and dying cells through efferocytosis cause chronic inflammation and autoimmune diseases (Boada-Romero et al., 2020). In addition to preventing the deleterious effects of secondary

necrosis, efferocytosis also couples corpse internalization to other environmental cues (such as local cytokines and metabolites) to temporally and spatially regulate macrophage anti-inflammatory and tissue repair functions (A-Gonzalez et al., 2017; Bosurgi et al., 2017; Perry et al., 2019). While the clearance of apoptotic cells is often associated with alternative macrophage programming, the identity of the dying cell, the type of cell death, and the context of death (either sterile or infectious) can modulate the nature of the macrophage response (Rothlin et al., 2020).

While infection with SARS-CoV2 induces the recruitment of immune cells to the lungs, their role in host defense and the causes for the dysfunction during disease progression remain elusive. Here, we sought to determine how macrophages operate when responding to dying epithelial cells infected with SARS-CoV-2. We found that the presence of viable SARS-CoV-2 in cell corpses dysregulates macrophage anti-inflammatory responses to the efferocytosis of apoptotic cells, promoting excessive production of inflammatory IL-6 and IL-1β while disrupting the efficient continual clearance of dead cells required for effective tissue repair. We also provide evidence that the expression of efferocytic genes is reduced in macrophages from severe COVID-19 patients. Therefore, SARS-CoV-2 infection and the clearance of infected dying cells disrupt macrophage host-protective functions associated with immunopathological manifestations of COVID-19.

Results

Macrophages engulf dying cells carrying viable SARS-CoV-2

SARS-CoV-2 infection causes cytopathic effects in human and primate epithelial cells (Chu et al., 2020; Zhu et al., 2020), possibly mediated by activation of multiple cell death pathways (Chan et al., 2020; Shaohua Li et al., 2020; Shufen Li et al., 2020; Mulay et al., 2021; Ren et al., 2020; Zhu et al., 2020). Notably, inhibition of apoptosis ameliorates cytokine expression and tissue damage in the lungs of SARS-CoV-2-infected mice, indicating that apoptosis in the lungs is pathogenic (Chu et al., 2021). Agreeing with previous reports (Chu et al., 2020; Ren et al., 2020; Zhu et al., 2020), infection with SARS-CoV-2 for 48 hours induced caspase-3 and caspase-8 activation in immortalized simian kidney epithelial Vero CCL81 (**Figure 1A)** and human lung epithelial Calu-3 cell lines **(Figures 1A** and **B)**. We also found features consistent with the predominance of apoptotic cell death at 48 h post-infection by flow cytometric analysis of the pattern of annexin V and a permeability dye co-staining in infected cells (**Figure 1C**). Consistently, we observed low levels of cytolysis in these infected cells, as assessed by lactate dehydrogenase release (**Figure 1D**). Immunofluorescent labeling of cleaved caspase-3 in lung tissues of deceased COVID-19 patients confirmed the induction of apoptosis in the epithelia infected with replicant SARS-CoV-2 (**Figure 1E**, and **Figure 1 – figure supplement 1A**). Examination of lung tissues also revealed evidence of macrophages with internalized epithelial cells and SARS-CoV-2, suggesting the uptake of infected epithelial cells by macrophages (**Figure 1F**).

We performed the Median Tissue Culture Infection Dose (TCID50) assay and found that viral particles obtained from isolated apoptotic Vero and Calu-3 cells induced cytopathic effect to an equivalent extent as those released in the culture supernatants (**Figure 1 – figure supplement**

1B). Furthermore, we isolated annexin V-labeled apoptotic cells (AC) from SARS-CoV-2-infected cell culture and confirmed that they carry viable viral particles **Figure 1G**). Therefore, viable SARS-CoV-2 is retained within infected, apoptotic epithelial cells.

Exposure of phosphatidylserine (PtdSer) on the outer plasma membrane of cells undergoing regulated cell death (RCD), as observed by annexin V binding to infected dying cells (**Figure 1C**), is the most ubiquitous signal that triggers their phagocytosis (Fadok et al., 1992; Nagata, 2018). To determine whether phagocytes efficiently engulf SARS-CoV-2-infected apoptotic cells (CoV2-AC), we collected the loosely attached apoptotic cells from infected cultures and used flow cytometry to assess their uptake by primary human macrophages and macrophages differentiated from THP-1 monocytes. We observed that macrophages efficiently engulf CoV2-AC, similarly to the uptake of sterile, UV-irradiated apoptotic cells (UV-AC) (**Figure 1H** and **Figure 1 – figure supplement 1C**). Analysis by confocal microscopy and staining for Spike protein confirmed the presence of SARS-CoV-2 in engulfed cell corpses (**Figure 1 – figure supplement 1D**). Finally, either stimulation with infected or sterile dying cells did not robustly affect macrophages viability up to 24 h post-treatment (**Figure 1 – figure supplement 1E**).

These results demonstrate that macrophages engulf cell corpses carrying viable particles of SARS-CoV-2, offering a framework to investigate their effects on macrophage function.

Efferocytosis of SARS-CoV-2-infected dying cells impairs macrophage anti-inflammatory function

We next addressed the effect of the engulfment of SARS-CoV-2-infected apoptotic cells in macrophages. The uptake of sterile apoptotic cells often promotes macrophage functional polarization toward an anti-inflammatory and tissue repair phenotype (Doran et al., 2020). We first observed that stimulation of primary monocyte-derived macrophages with CoV2-AC, but not infection with SARS-CoV-2, reduced the expression of genes associated with alternative programming to tissue remodeling and secretion of immune-modulatory mediators such as *CCL18*, *CD206* (also known as *MRC1*), *MMP9*, *PPARG* and *CD163* (**Figure. 2A**). Furthermore, stimulation with UV-AC obtained from infected Vero cells increased both gene (**Figure 2A**) and surface protein (**Figure 2B, Figure 2 – figure supplement 1A**) expression of the anti-inflammatory marker CD206. However, upregulation of MRC1 at the gene or protein levels did not occur in response to stimulation with CoV2-AC (**Figures 2A** and **B**). We obtained similar results in THP-1-derived macrophages stimulated with CoV2-AC obtained from either Calu-3 or Vero cells infected with SARS-CoV-2 (**Figure 2 – figure supplement 1B-D**). Stimulation with the conditioned supernatants of infected dying cells (containing putative DAMP, cytokines produced by epithelial cells, extracellular vesicles, and released virions) or direct infection with SARS-CoV-2 did not induce *MRC1* transcription (**Figure 2A, Figure 2 – figure supplement 1B**) or surface expression (**Figure 2B, Figure 2 – figure supplement 1C** and **D**) in macrophages. We also confirmed that modulation of CD206 expression occurred specifically in the macrophages that engulfed apoptotic cells and was not due to paracrine signaling (**Figure 2C** and **Figure 2 – figure supplement 1E**). To determine if viral viability was required to modulate CD206 expression by infected apoptotic cells, isolated CoV2-AC were exposed to UV irradiation for virus inactivation (**Figure 2 – figure supplement 1F**). Notably, macrophages treated with epithelial AC containing inactivated SARS-CoV-2 exhibited increased CD206

surface expression, similar to that of UV-AC (**Figure 2D**). This finding suggests that viable SARS-CoV-2 actively represses alternative programming carried in dying cells and is not primarily enforced by the type of cell death caused by the infection. Efferocytosis of sterile UV-AC in the presence of SARS-CoV-2 still induced higher expression of CD206 in macrophages (**Fgure 2E**). Therefore, the suppression of CD206 surface expression required delivery of viral particles within cell corpses to macrophages.

Conversely, the uptake of CoV2-AC, but not UV-AC, significantly increased *IL6* expression in monocyte- and THP-1-derived macrophages (**Figure 3A** and **Figure 3 – figure supplement 1A**, respectively). The uptake of CoV2-AC also induced robust secretion of inflammatory IL-6 and IL-1β, in both primary (**Figure 3B**) and THP-1-derived macrophages (**Figure 3 – figure supplement 1B** and **C**). We did not detect these cytokines in macrophages stimulated with the cell-free conditioned supernatants (**Figure 3B** and **Figure 3 – figure supplement 1A-C**), and therefore this effect was not due to immune mediators or viral particles released from infected epithelial cells. Importantly, assessment of IL-6 secretion in macrophages stimulated with sorted out populations of infected dying cells revealed that cytokine production occurred specifically in response to apoptotic cells, but not permeabilized dead cells (**Figure 3C**). In agreement, CoV2-AC obtained from epithelial cells infected in the presence of osmoprotectant glycine, which non-specifically prevents the leak of cytosolic content by lytic permeabilization (Evavold et al., 2017; Frank et al., 2000) still induced robust secretion of IL-6 by macrophages (**Figure 3 – figure supplement 1D**).

Further, the induction of inflammatory cytokines by SARS-CoV-2-loaded corpses required the presence of viable viral particles, as UV-treatment or paraformaldehyde-fixation of isolated CoV2-AC abrogated IL-6 secretion (**Figure 3D**). Notably, we did not observe robust production of IL-6 in response to dying epithelial cells infected with Coxsackievirus (**Figure 3 – figure supplement 1E** and **Figure 3E**). This result suggests that augmented pro-inflammatory cytokine production is not a universal response of macrophages to the uptake of cell corpses infected with positive single-strand viruses.

To confirm the requirement of recognition and binding of CoV2-AC to promote inflammatory skewing, we stimulated macrophages in the presence of annexin V to mask PtdSer exposed on the surface of the apoptotic cells. In the absence of PtdSer ligation, macrophages did not secrete IL-6 in response to CoV2-AC (**Figure 3F** and **Figure 3 – figure supplement 1F**). Stimulation of macrophages in the presence of actin depolymerization inducer Cytochalasin D, which allows corpse binding but not internalization, also attenuated IL-6 production (**Figure 3G**). Finally, we tested the effect of antiviral drugs targeting viral RNA transcription (RdRP-mediated RNA synthesis). We found that Remdesivir treatment of primary macrophages following stimulation with CoV2-AC partially reduced IL-6 secretion, suggesting that viral sgRNA expression is important to modulate the inflammatory response (**Figure 3H**).

Collectively, these findings support that sensing and engulfment of dying cells carrying viable SARS-CoV-2 switch macrophage anti-inflammatory, resolutive programming in response to efferocytosis toward an inflammatory phenotype. The exacerbated cytokine production observed

in response to the efferocytosis of infected cell corpses by macrophages may contribute to the cytokine storm associated with COVID-19 hyperinflammatory syndrome.

Efferocytosis of SARS-CoV-2-infected dying cells suppresses continual clearance of apoptotic cells

Several receptors mediate efferocytosis through recognition of PtdSer on the surface of a dying cell, either by direct binding or through a bridging molecule (Boada-Romero et al., 2020; Penberthy and Ravichandran, 2016). We found that engulfment of CoV2-AC by primary macrophages reduced the transcription of such PtdSer receptors, including the scavenger receptors *CD36* and *SRA1*, αVβ5 integrin (*ITGB5*), and T cell immunoglobulin mucin receptor 4 (*TIM4*) and MER proto-oncogene tyrosine kinase (*MERTK*) (**Figure 4A**). In THP-1-macrophages, we also observed reduced expression of *SRA1, ITGB5,* and *TIM4* receptors in response to infection with SARS-CoV-2 (**Figure 4 – figure supplement 1A**). Phagocytes can ingest multiple corpses in subsequent rounds of efferocytosis (Miyanishi et al., 2007; Morioka et al., 2018; Park et al., 2011; Yurdagul et al., 2020). Previous *in vivo* work showed that macrophages must continually remove ACs to promote efficient repair of injury and prevent the accumulation of secondarily necrotic cells (Wang et al., 2017; Yurdagul et al., 2020). To determine if repression of efferocytic receptors affects additional uptake of dying cells, we treated macrophages with CoV2-AC and subsequently fed them with apoptotic human Jurkat cells (UV-Jurkat). We found that the engulfment of SARS-CoV-2-infected corpses suppressed the efferocytosis of other apoptotic cells (**Figure 4B-E, Figure 4 – figure supplement 1B**). As infection with SARS-CoV-2 reduced the expression of some efferocytic receptors in THP-1

macrophages (**Figure 4 – figure supplement 1A**), we also tested if it affected the uptake of apoptotic cells. Comparatively, infection with SARS-CoV-2 reduced AC clearance to a lower extent than prior uptake of CoV2-AC (**Figure 4 – figure supplement 1C**). Notably, treatment with Remdesivir did not improve the subsequent uptake by macrophages stimulated with CoV2-AC, arguing that viral RNA replication is not required for suppression of efferocytosis in response to CoV2-AC (**Figure 4F**). This result also suggests that different mechanisms lead to pro-inflammatory cytokine production and efferocytosis repression in response to the uptake of infected corpses.

Thus, efferocytosis of SARS-CoV-2-infected dying cells affects the expression of efferocytic receptors and impairs the continual removal of apoptotic cells by macrophages.

Lung monocytes and macrophages of severe COVID-19 patients express reduced levels of efferocytic receptors

To gain insight into the contribution of dysfunctional efferocytosis in COVID-19 pathogenesis, we assessed the expression of efferocytic receptors by immunofluorescence in lung tissues obtained from autopsies of deceased COVID-19 patients. We found a reduction in the protein levels of CD36 in $S1009^{+}$ infiltrating phagocytes in the lungs of COVID-19 patients compared to control tissues (**Figure 5A**). Phagocytes in the lungs of COVID-19 patients also expressed lower protein levels of MERTK (**Figure 5B**).

Using publicly available single-cell RNA sequencing (scRNA-seq) data from bronchoalveolar lavage (BAL) (Liao et al., 2020), we performed enrichment analysis using the genes differentially expressed (DEG) in mild and severe COVID-19 patients compared with healthy individuals. We targeted efferocytosis-related gene ontology (GO) annotated pathways and customized gene sets based on the literature (Boada-Romero et al., 2020; Penberthy and Ravichandran, 2016) (**Supplementary File 1**). Independent analysis of clusters previously assigned as macrophages (Liao et al., 2020) revealed significant repression of gene sets related to efferocytosis in severe patients (**Figure 5C**). While differences were evident between moderate and severe patients were observed in clusters expressing markers of early infiltrating phagocytes ($S1009^{+}$ $CCL18^{-}$), they were more pronounced in mature, likely anti-inflammatory macrophages ($S11009^{-}$ $CCL18^{+}$). Notably, reassessment on scRNAseq by Ren et al. (2021) showed enrichment in pathways related to efferocytosis for genes repressed in alveolar macrophages which were positive for SARS-CoV-2 RNA compared with those which were negative to the virus (**Figure 5D**). This finding is consistent with the notion that uptake of infected cells reduces the capacity of macrophages to clear other dead cells. Altogether, these data support that macrophages in the lungs of severe COVID-19 patients may also fail in their efferocytic capacity.

Discussion

Patients with severe COVID-19 develop life-threatening inflammatory process in the lungs with underlying causes still not established. Here, we demonstrate that the sensing and engulfment of SARS-CoV-2-infected dying cells by macrophages switches the effector response to

efferocytosis from a potential wound healing, anti-inflammatory function to a pro-inflammatory one. Our data supports that the uptake of cell corpses infected with SARS-CoV-2 exacerbates the secretion of inflammatory IL-6 and IL-1β, suggesting a mechanism for the robust secretion of cytokines related to COVID-19 cytokine storm. Another important consequence of this shift in macrophage function is the impairment of macrophage capacity to engulf apoptotic cells continually and promote proper injury resolution. Instead, our data suggest that efferocytosis of infected cells may augment tissue damage by causing inefficient clearance of dead cells. This process may consequently contribute to respiratory complications developed by patients with the severe form of the disease and increase susceptibility to secondary bacterial infections for the lack of effective disease tolerance mechanisms that restrain collateral tissue damage (Jamieson et al., 2013). While such causal connection remains to be investigated, our histological assessment and reanalysis of scRNAseq datasets suggest that the efferocytic capacity of lung macrophages is impaired in the lungs of COVID-19 patients.

In the context of COVID-19 immunopathogenesis, excessive amounts of necrotic cells may lead to high levels of circulating DAMP, such as HMGB1 and lactate dehydrogenase (LDH), both of which correlate with disease severity (Chen et al., 2020; Han et al., 2020; Rodrigues et al., 2020). It is thus possible that the combination of exacerbated cytokine production and interruption of continual efferocytosis in response to engulfment of SARS-CoV-2-infected corpses could both increase the magnitude and duration of inflammation, contributing to the hyperinflammatory state and multiorgan damage in COVID-19. Finally, some studies reported higher levels of autoantibodies (such as against IFNγ, phospholipids, and annexin A2) in COVID-19 patients (Bastard et al., 2020; Zuniga et al., 2021; Zuo et al., 2020), suggesting that autoantibodies may

drive the worsening of the disease. It has long been known that defective engulfment or processing of dying cells causes the development of autoimmune diseases (Boada-Romero et al., 2020; Cohen et al., 2002; Miyanishi et al., 2007; Peng and Elkon, 2011; Rodriguez-Manzanet et al., 2010). In light of our findings, perhaps defective clearance of apoptotic cells caused by SARS-CoV-2 infection and SARS-CoV-2-loaded ACs also contributes to COVID-19-associated autoimmunity.

As it becomes clear that worsening of COVID-19 occurs because of immune dysfunction, antivirals, and other therapeutic efforts to limit viral replication may fail to benefit critically ill patients. In those patients, successful therapeutic strategies may rely on targeting dysregulated components of the host response to limit damage to the host, thus promoting disease tolerance and stimulating a resolutive response that restores homeostasis. In this context, our study provides important insights into the mechanisms driving the pathophysiology of COVID-19 that can be explored in the design of therapeutics approaches toward harnessing innate immune responses and macrophage function during the evolution of SARS-CoV-2 infection.

Material and Methods

Study approval. The procedures followed in the study were approved by the Research Ethics Committee of Hospital das Clínicas de Ribeirão Preto (CEP-FMRP/USP) and by the National Ethics Committee, Brazil (Comissão Nacional de Ética em Pesquisa (CONEP), protocols 30248420.9.0000.5440 and 39722020.9.0000.5440. Written informed consent was obtained from recruited donors.

Isolation of human peripheral blood mononuclear cells, monocyte seeding, and macrophage differentiation. Peripheral blood mononuclear cells (PBMC) from healthy donors were isolated from peripheral blood. The samples were centrifuged at 400 *g* for 10 min at room temperature (RT), the plasma was discarded, and the cellular portion was diluted in phosphate-buffered saline (PBS). PBMC were isolated by density–gradient centrifugation using Histopaque-1077 (Sigma-Aldrich). The collected PBMC fraction was treated with ACK lysis buffer to lyse erythrocytes and washed twice with PBS. For macrophages differentiation, monocytes were cultivated for 7 d in RPMI 1640 media supplemented with penicillin (10.000 U/mL, GIBCO), streptomycin (10.000 µg/mL, GIBCO), 1% glutamine (GIBCO), and 10% heat-inactivated human serum (Sigma Aldrich) at 37°C in a 5% CO_2 atmosphere.

Cell Lines. Calu-3 and Jurkat cells were originally from (ATCC®) and purchased from Banco de Células do Rio de Janeiro (BCRJ). Vero CCL81 and THP-1 cells were from Dario Zamboni's lab. No authentication method was used. Calu-3 and Vero CCL81 cells were maintained in DMEM with 4.5 g/L glucose (GIBCO) supplemented with penicillin (10,000 U/mL), streptomycin (10,000 µg/mL), and 10% heat-inactivated fetal bovine serum (FBS, GIBCO) (DMEMc) at 37°C in a 5% CO_2 atmosphere. Jurkat cells and THP-1 cells were maintained in RPMI1640 media supplemented with penicillin (10,000 U/mL), streptomycin (10,000 µg/mL), 1% glutamine, and 10% FBS (RPMIc) at 37°C in a 5% CO_2 atmosphere.

THP-1-derived macrophages were obtained by treatment with phorbol 12-myristate 13-acetate (PMA, 50 ng/mL, Sigma-Aldrich) for 24 h, followed by media replenishment with fresh RPMIc and other 24 h incubation period before stimulation.

Cell lines were routinely screened by PCR for mycoplasma contamination, and all cell lines tested negative.

Viral stock. The SARS-CoV-2 strain (Brazil/SPBR-02/2020) was isolated from the first Brazilian case of COVID-19. The viral stock was produced in a monolayer of Vero CCL81 cells expressing ACE2 (Rodrigues et al., 2020), maintained in serum-free DMEM at 37°C in a 5% CO_2 atmosphere. Coxsackievirus B5 (Coxsackie) was originally shared by Dr. Roger M. Loria (Virginia Commonwealth University, Richmond, Virginia, USA) (Gomes et al., 2009). The viral stock was produced in a monolayer of HeLa cells maintained in DMEM supplemented with 2% FBS at 37°C and 5% CO_2. Viral stocks were propagated under BSL3 conditions and stored at -80°C. Viral loads were estimated by titration in Vero CCL81 cells seeded onto 96-well plates and standard limiting dilution to confirm the 50% tissue culture infectious dose.

Infection and UV-irradiation of epithelial cell lines. Cell monolayers were rinsed with PBS, replenished with a thin layer of serum-free media, and infection with a freshly thawed virus aliquot at a multiplicity of infection (MOI) of approximately 0.05 was carried out for 1 h at 37°C and 5% CO_2 for viral adsorption. The cells were then topped with fresh media and incubated for 48 h. Sterile apoptotic cells (UV-AC) were generated by exposure to UV-C radiation (Calu-3 cells at 500 mJ/cm^2 and Vero CCL81 cells at 350 mJ/cm^2) in a UV crosslinker (Fisher Scientific), followed by 6h incubation in DMEMc at 37°C and 5% CO_2.

386 **Cell death assays**. Cells were collected 48 hours post-infection or 6 hours post-irradiation, spun
387 at 300 *g* for 5 min, washed with PBS, and resuspended in the appropriate buffer before analysis.
388
389 For the analysis of caspase-8 and caspase-3 cleavage, 2.0 x 10^6 Vero CCL81 and Calu-3 cells
390 stimulated as described were lysed in RIPA buffer (10 mM Tris-HCl, pH 7.4, 1 mM EDTA, 150
391 mM NaCl, 1% Nonidet P-40, 1% deoxycholate, and 0.1% SDS) supplemented with protease
392 inhibitor cocktail (Sigma). Precleared lysates were quantified by Bradford assay, boiled in
393 Laemmli buffer, resolved by SDS-PAGE and transferred to PVDF membranes. Rabbit anti-
394 cleaved caspase-3/caspase-3/cleaved Caspase-8/caspase-8 (all from Cell Signaling), rabbit anti-
395 SARS-CoV-2 Spike (Abcam), HRP-conjugated goat anti-actin (Cell Signaling), and species-
396 specific horseradish-conjugated secondary antibodies were used for antigen detection.
397
398 For the analysis of cleaved caspase-3 by flow cytometry, infection of Calu-3 cells was carried
399 out in the presence of Z-VAD-FMK (Selleckchem) at 20 μM, or mock treatment with vehicle
400 (DMSO), added to cell cultures after virus adsorption. 10^6 collected cells were washed with PBS,
401 and fixation, permeabilization, and staining were carried out using BD Cytofix/Cytoperm™
402 Fixation/Permeabilization Kit (BD Biosciences), following the manufacturer's instructions.
403 Samples were incubated with rat serum (1:400) for 5 min at RT followed by immunolabelling of
404 intracellular active caspase-3 was performed with anti-cleaved caspase-3 (Cell Signaling, 1:400)
405 and secondary donkey anti-rabbit IgG conjugated to Alexa Fluor 488 (Thermo Fisher Scientific,
406 1:2,500). Sample acquisitions were performed in a FACSVerse™ (BD Biosciences) flow
407 cytometer and data processing was performed using FlowJo_V10 software (BD Biosciences).
408

Cell death profiling in infected or UV-irradiated Vero CCL81 cells was performed with a viability dye (Zombie NIR™ Fixable Viability Dye, Biolegend, 1:400) and annexin V (FITC annexin V, BD Biosciences, 1:200) co-labeling. Labeling of 1.0 x 10^6 cells with Zombie NIR was carried out for 10 min on ice, followed by annexin V labeling for 15 min on ice with cells resuspended annexin V binding buffer (0.01M HEPES, 0.14M NaCl, 2.5 mM $CaCl_2$, pH 7.4). Sample acquisitions were performed in a in a BD FACSMelody™ (BD Biosciences) cell sorter and data processing was performed using FlowJo_V10 software (BD Biosciences).

To determine LDH release, infection or UV-irradiation of 2.0 x 10^5 Vero CCL18 cells were carried out in DMEMc without Phenol Red. LDH release was measured in the culture supernatants using the CytoTox 96 Non-Radioactive Cytotoxicity Assay (Promega), following the manufacturer's instructions.

Isolation of apoptotic cells. Apoptotic cells were generated from SARS-CoV-2-infected (CoV2-AC) or UV-irradiated (UV-AC) Vero CCL81 and Calu-3 cells, or Coxsackievirus B5-infected Vero CCL81 cells (Coxsackie-AC). At the established time points, the supernatants were collected and temporarily stored for further processing. Then, a suspension containing CoV2-AC, Coxsackie-AC or UV-AC was obtained by carefully pipetting fresh media up and down the plate surface and collecting loosely attached cells. Following spun at 300 *g* for 5 min, pelleted AC were washed with PBS, resuspended in RPMIc, and counted prior to incubation with macrophages. Enrichment in apoptotic cells were confirmed by annexin V staining and flow cytometry.

To sort CoV2-AC populations, annexin V^+ cells were pre-enriched using magnetic separation (Annexin V MicroBead Kit, Miltenyi Biotec) following the manufacturer's instructions. Then cells were labeled with Zombie NIR and annexin V-FITC, as described above, and cell sorting were performed in a BD FACSMelody™ (BD Biosciences) cell sorter. Isolated CoV2-AC were washed in PBS, resuspended in fresh RPMIc, and counted prior to incubation with macrophages

For virus inactivation, isolated CoV2-AC suspension was placed onto tissue culture hood surface with an open lid for 20 min with the UV-C lamp on. Virus inactivation was confirmed by $TCID_{50}$, as described below. Alternatively, isolated AC were fixed with 2% paraformaldehyde (PFA) in PBS for 10 min and washed twice with PBS before adding to macrophage cultures.

To prepare the cell-free conditioned supernatants of the infected AC (CoV2-AC Sup), collected supernatants were spun at 300 *g* for 5 min to remove cellular debris; the resulting supernatant was filtered using a 0.22 μm syringe filter and immediately used for macrophage stimulation. The volume of CoV2-AC Sup used to stimulate macrophages was normalized to the amount of collected AC.

$TCID_{50}$ quantification of viable viral particles. 1.0×10^6 isolated CoV2-AC and their equivalent purified conditioned supernatants, obtained as described above, were lysed by snap freeze-and-thaw. To estimate viral load in apoptotic cells isolated by annexin V labeling, all infected cells were collected, followed by magnetic separation with annexin V MicroBeads (Miltenyi Biotec) according to the manufacturer's protocol. 1.0×10^6 pre-sorted cells and annexin$^+$ cells were lysed by freeze-and-thaw for quantification. Viral loads were estimated by

titration in Vero CCL81 cells seeded onto 96-well plates and expressed as 50% tissue culture infectious dose ($TCID_{50}$). Quantification was performed with the Reed-Muench method and plotted as $TCID_{50}$ units per mL (Reed and Muench, 1938).

***In vitro* assays with THP-1- and PBMC-derived macrophages.** 1.0 x 10^6 THP-1- and PBMC-derived macrophages seeded on 24-well tissue culture plates were rinsed with warm PBS before stimulation. Macrophage cultures were then topped with UV-AC, CoV2-AC, or Coxsackie-AC resuspended in the appropriate serum-containing macrophage media at a 1:1 ratio. Macrophage cultures were rinsed out 2 h after incubation to remove unbound AC and topped with fresh media at the indicated time points, cell supernatants were collected and macrophages were rinsed at least twice with warm PBS to remove cell debris before proceeding to further analysis. To block AC ligation and efferocytosis, CoV2-AC were pre-incubated with 0.1 or 0.01 µg/mL of annexin-V (BD Biosciences) and macrophage stimulation was carried out in RPMIc supplemented with Ca^{2+}. To block AC internalization, macrophages were pre-treated for 30 min, and incubation was carried out in the presence of Cytochalasin D (10 µM, Sigma). Where indicated, macrophages were topped with fresh media containing Remdesivir (20 µM, BOC Sciences) after removal of unbound AC.

For stimulation with conditioned supernatants, CoV2-AC-Sup were added directly to macrophages cultures and topped with fresh media for volume adjustment. Infection with SARS-CoV-2 or Coxsackie virus was carried out with virus adsorption at MOI 0.1 in serum-free media for 1 h before topping with fresh serum-containing media.

For gene expression analysis by RT-qPCR, rinsed macrophage cultures were lysed in Trizol (Thermo Scientific) and immediately frozen at -80°C.

To estimate CD206 surface expression, rinsed macrophages were removed with a cell scraper, spun at 300 *g* for 5 min, washed with PBS, followed by incubation with rat serum (1:400) for 5 min at RT and cell surface staining for 15 minutes at 4°C. Cells were labeled with Zombie Violet™ Fixable Viability Kit (Biolegend) and anti-CD206-FITC antibody (clone 19.2, BD Biosciences). The cells were then fixed with 2% PFA for 10 min and washed before flow cytometric analyses in a FACSVerse (BD Biosciences) flow cytometer and data processing was performed using FlowJo_V10 software (BD Biosciences).

For immunofluorescence imaging of efferocytosis in vitro, human monocyte-derived macrophages seeded onto 13mm round coverslips were incubated with UV-AC or CoV2-AC labeled with 5 µM CellTrace™ CFSE dye (Thermo Scientific) for 2 h. After rinsing out non-engulfed AC, macrophages were fixed for 20 min with PBS 2% PFA at RT. Cells were then permeabilized with 0.1% Triton-X-100 in PBS for 10 min at room temperature RT. Next, cells were rinsed twice in PBS and incubated with PBS 1% bovine serum albumin (BSA) and 5 µg/mL normal donkey IgG (Jackson ImmunoResearch) for 45 min RT prior to overnight (ON) incubation at 4ºC with primary antibodies: rabbit polyclonal anti-SARS-CoV-2 Spike antibody (Abcam, 1:1,000) and mouse mAb anti-rat CD11b (Abcam, 1:300) diluted in PBS containing 1% BSA. Next, cells were rinsed thoroughly in PBS and incubated for 30 min at RT with the secondary antibodies diluted in PBS: Alexa-594 goat-anti rabbit IgG (1:1,000; Thermo Scientific) and Alexa-647 donkey-anti mouse IgG (1:1,000; Thermo Scientific). Cell nuclei were

stained with Hoechst 33342. Cells were then rinsed, and coverslips mounted on glass slides with Fluoromount-G (Invitrogen). Samples were imaged using a Zeiss LSM 780 laser scanning confocal microscope (Carl Zeiss), postprocessed for brightness and contrast adjustment with ImageJ image processing package (NIH) and layouts were built on Adobe Photoshop.

For the engulfment assays by flow cytometry, macrophages were labeled with 5 µM CellTrace™ Violet dye (CTV, Thermo Scientific), according to the manufacturer's recommendations. CellTrace™ Violet (CTV)-labeled macrophages were stimulated with UV-AC or CoV2-AC previously stained with 1 µM CellTrace™ Far Red dye (CTFR, Thermo Scientific), or 5 µM CellTrace™ CFSE dye, as described in the legend of the figures. Following the removal of unbound AC, macrophages were collected with a cell scraper, fixed with 2% PFA for 10 min, and washed before proceeding with the acquisition by flow cytometry. For the two-round efferocytosis assay, first-round UV-AC and CoV2-AC were labeled with a pH indicator fluorogenic intracellular probe (pHRodo Red AM Intracellular pH Indicator - Thermo Scientific). Second-round apoptotic Jurkat cells (UV-Jurkat) were generated by labeling with 1 µM CTFR and UV-C irradiation at 20 mJ/cm^2, followed by incubation at 37°C and 5% CO_2 for 6 h. CTV-labeled THP-1 cells were incubated with pHrodo-UV-AC or pHrodo-CoV2-AC for 18h at a 1:1 ratio. Cells were then rinsed with PBS, and CTV-labeled UV-Jurkat were added to the culture at a 1:1 ratio for 2h. Macrophage cultures were collected with a cell scraper, washed, fixed with 2% PFA for 10 min, and washed before proceeding with the acquisition by flow cytometry. Flow cytometric acquisition was performed in a FACSVerse (BD Biosciences) flow cytometer and data processing was performed using FlowJo_V10 software (BD Biosciences).

Cytokine quantification. IL-6 and IL-1β cytokine levels in macrophage supernatants were evaluated by ELISA assay (R&D Systems) or Cytometric Bead Array (CBA, BD Biosciences), as indicated in the legend of the figures, following the manufacturers' recommendations.

RNA isolation and gene expression analyses. Total RNA extraction for human monocyte- or THP-1-derived macrophages stimulated *in vitro* was performed using Directzol™ RNA miniPrep Kit (Zymo Research), following the manufacturer's recommendations. Reverse transcriptase was performed using M-MLV reverse transcriptase (Thermo Scientific) according to the manufacturer's recommendations.

Gene expression RT-qPCR was performed using SybrGreen Master Mix (Applied Biosystems). RT-qPCR was performed in fast mode, following the manufacturer's recommendations. The evaluation of each gene expression was determined by the comparative CT method. Primer sequences used were:

Gene	5' Forward	3' Reverse
CCL18	CTCTGCTGCCTCGTCTATACCT	CTTGGTTAGGAGGATGACACCT
CD163	GCGGGAGAGTGGAAGTGAAAG	GTTACAAATCACAGAGACCGCT
CD36	GGGAAAGTCACTGCGACATG	TGCAATACCTGGCTTTTCTCA
GAPDH	GTCTCCTCTGACTTCAACAGCG	ACCACCCTGTTGCTGTAGCCAA
IL6	GGTACATCCTCGACGGCATCT	GTGCCTCTTTGCTGCTTTCAC
ITGB5	AACCAGAGCGTGTACCAGAA	AGGAGAAGTTGTCGCACTCA
MERTK	CTCTGGCGTAGAGCTATCACT	AGGCTGGGTTGGTGAAAACA
MMP9	TGTACCGCTATGGTTACACTCG	GGCAGGGACAGTTGCTTCT
MRC1	AGCCAACACCAGCTCCTCAAGA	CAAAACGCTCGCGCATTGTCCA
PPARG	ACCAAAGTGCAATCAAAGTGGA	ATGAGGGAGTTGGAAGGCTCT
SRA1	GCAGTGGGATCACTTTCACAA	AGCTGTCATTGAGCGAGCATC
TIM4	ACAGGACAGATGGATGGAATA CCC	AGCCTTGTGTGTTTCTGCG

Histological analysis. Ultrasound-guided minimally invasive autopsies for COVID-19 deceased patients were approved by the Research Ethics Committee of Hospital das Clínicas de Ribeirão Preto (CEP, protocol no. 4.089.567). **Supplementary File 2** describes clinical, laboratory, and treatment records of COVID-19 patients. Non-neoplasic sections of lung parenchyma were obtained from lobectomies for lung cancer as a control group (Rodrigues et al., 2020). Paraffin sections from lungs were collected and processed as previously described (Rodrigues et al., 2020). Sections were rinsed in PBS, and the antigen retrieval was performed by incubation of samples with 0.1% trypsin (ThermoFisher Scientific) in PBS at 37ºC for 15 min. Next, sections were rinsed and incubated with Image-iT FX Signal Enhancer (ThermoFisher Scientific) for 30 min at RT. Sections were then rinsed in PBS and incubated for 45 min at RT in PBS containing 0.5% BSA and 5µg/mL normal donkey IgG (Jackson ImmunoResearch).

For analysis of active caspase-3, lung sections were labeled with primary antibodies diluted in PBS and incubated overnight at 4ºC: rabbit polyclonal anti-human cleaved caspase-3 (Asp175) (Cell Signaling; 1:1,000) and mouse anti-dsRNA (SCICONS; 1:1,000). Then, sections were rinsed thoroughly in PBS and incubated for 45 min at RT with the secondary antibodies: Alexa 594 goat anti-rabbit IgG (1:500; Thermo Fisher Scientific) and Alexa 488 goat anti-mouse IgG F(ab)´$_2$ (1:500; Thermo Fisher Scientific) diluted in PBS. Cell nuclei were stained with Hoechst 33342. Cells were then rinsed, and coverslips mounted on glass slides with Fluoromount-G (Invitrogen). For *in situ* efferocytosis analysis, lung sections were labeled with primary antibodies mouse mAb anti-human CD68 (Abcam; 1:100), rabbit mAb anti-human cytokeratin 18 (GeneTex, 1:500) diluted in PBS and incubated overnight at 4ºC. Then, sections were rinsed thoroughly in PBS and incubated for 45 min at RT with the secondary antibodies F(ab)'$_2$ goat

anti-mouse IgG conjugated to Alexa 488 (1:500; Thermo Scientific) and goat anti-rabbit IgG conjugated to Alexa 647 (1:500; Thermo Scientific). Next, sections were rinsed in PBS and incubated overnight at 4ºC with rabbit polyclonal anti-SARS-CoV-2 Spike (Abcam; 1:1,000) previously conjugated to Alexa 568, according to the manufacturer's instructions (Zenon Alexa Fluor 568 Rabbit IgG Labeling Kit, Thermo Scientific). Sections were then rinsed in PBS and incubated for 15 min at RT with Hoechst 33342 (Invitrogen), rinsed thoroughly, and mounted on glass slides with Fluoromount-G (Invitrogen). Samples from Cl-caspase-3 and in situ efferocytosis experiments were imaged using an ECLIPSE Ti2 Series microscope equipped with a DS-Qi2 camera (Nikon Instruments Inc.). Analysis was performed using NIS Elements (Nikon Instruments Inc.), wherein mean intensity fluorescence for Cl-caspase-3 was determined for randomly selected epithelial cells. Representative images were postprocessed for brightness and contrast adjustment with ImageJ image processing package (NIH) and layouts were built on Adobe Photoshop.

For CD36 or MERTK expression analysis, lung sections were labeled with the primary antibodies diluted in PBS and incubated overnight at 4ºC: rabbit polyclonal anti-human CD36 (PA5-81996; 1:100 ThermoFisher Scientific) or rabbit mAb anti-human MERTK (Clone SR29-07; 1:150; ThermoFisher Scientific) and mouse mAb anti-human calprotectin (Clone MAC387; MA1-81381; 1:100; ThermoFisher Scientific). Then, sections were rinsed thoroughly in PBS and incubated for 45 min at RT with the secondary antibodies Alexa 488 donkey anti-rabbit IgG (1:500; Thermo Fisher Scientific) and Alexa 594 goat anti-mouse IgG (Thermo Scientific) diluted in PBS. Sections were then rinsed, and coverslips mounted with DAPI Fluoromount-G. Samples were imaged using an Olympus BX61 Fluorescence Motorized Slide Scanner

586 Microscope Pred VS120 (Olympus). Analysis was performed using ImageJ image processing
587 package (NIH), wherein mean intensity fluorescence for CD36 and MERTK was determined for
588 randomly selected S1009^{+} cells. Representative images were postprocessed for brightness and
589 contrast adjustment with ImageJ image processing package (NIH) and layouts were built on
590 Adobe Photoshop.
591
592 **Re-analysis of scRNA-seq Data**. We re-analyzed single-cell transcriptomic data from
593 bronchoalveolar lavage fluid (BAL) from patients with varying severity of COVID-19 disease
594 and their respective healthy controls (Liao et al., 2020). The dataset is publicly available at
595 https://covid19-balf.cells.ucsc.edu/. Downloaded data was imported into R environment version
596 v3.6.3. Differential expression analysis was conducted using FindMarkers function in Seurat
597 using the Wilcoxon test to compare mild and severe COVID-19 patients with healthy individuals
598 for each cluster previously identified by authors. Differentially expressed genes between
599 mild/severe COVID-19 patients and controls for each cluster were identified considering genes
600 expressed in at least 5% of cells and FDR < 0.05 and |avg_logFC| > 0.1. In addition, a
601 differentially expressed gene list comparing infected (identified SARS-Cov-2 transcripts) against
602 non-infected alveolar macrophages were obtained from supplemental materials from (Ren et al.,
603 2021). Gene Set Enrichment Analysis (GSEA) was performed using ClusterProfiler and fgsea R
604 packages (Korotkevich et al., 2021; Wu et al., 2021) for each differentially expressed gene or
605 log2 fold-change lists from Liao et al. (2020) and Ren et al. (2021) dataset. A custom gene set
606 was also utilized as a reference for GSEA, incorporating GO:0006911, GO:0043277 gene
607 ontology terms, and additional efferocytic related genes from the literature (Penberthy and

608 Ravichandran, 2016; Boada-Romero et al., 2020) (**Table S1**). Significantly enriched sets were
609 identified considering terms with p-value < 0.05.
610
611 **Quantification and statistical analyses.** Please refer to the legend of the figures for description
612 of samples, sample sizes (biological replicates) and experimental replicates. No statistical tests
613 were used to estimate sample size. Data were plotted and analyzed with GraphPad Prism 8.4.2
614 software (GraphPad Prism Software Inc., San Diego, CA). The statistical tests used are listed in
615 the legend of the figures. For the *in vitro* assays, we used Student's t-test to compare two
616 experimental groups or ANOVA and multiple comparison correction, to compare three or more
617 experimental groups. For quantification of histological datasets, normality tests were performed,
618 and samples with non-Gaussian distribution were analyzed applying the Mann–Whitney test.
619
620 **Acknowledgements**
621 The authors thank Dr. Denise M. da Fonseca, Msc. Elizabete R. Milani and Dr. Roberta
622 R. C. Rosales (FMRP-USP) for technical assistance.
623
624 **Funding**: This work was supported by grants from:
625 Fundação de Amparo a Pesquisa do Estado de São Paulo (FAPESP) grants
626 2018/25559-4 and 2020/05288-6 (L.D.C)
627 Coordenação de Aperfeiçoamento de Pessoal de Nível Superior (CAPES) grant
628 88887.507253/2020-00 (D. S. Z. and L.D.C.)
629 Conselho Nacional de Desenvolvimento Científico e Tecnológico (CNPq) grant
630 434538/2018-3 (L.D.C.)

D. S., A. C. G. S., T. S. R., M. F. R., E. G. F. F., D. L. A. T. are supported by FAPESP fellowships.

Competing Interests

The authors declare no competing financial interests.

Data Availability

All data are available in the main text or supporting information.

References

A-Gonzalez N, Quintana JA, García-Silva S, Mazariegos M, Aleja AG de la, Nicolás-Ávila JAA, Walter W, Adrover JM, Crainiciuc G, Kuchroo VK, Rothlin CV, Peinado H, Castrillo A, Ricote M, Hidalgo A. 2017. Phagocytosis imprints heterogeneity in tissue-resident macrophages. *The Journal of experimental medicine* 214:1281–1296. doi:10.1084/jem.20161375

Banerjee S, Friggeri A, Liu G, Abraham E. 2010. The C-terminal acidic tail is responsible for the inhibitory effects of HMGB1 on efferocytosis. *J Leukocyte Biol* 88:973–979. doi:10.1189/jlb.0510262

Bastard P, Rosen LB, Zhang Q, Michailidis E, Hoffmann H-H, Zhang Y, Dorgham K, Philippot Q, Rosain J, Béziat V, Manry J, Shaw E, Haljasmägi L, Peterson P, Lorenzo L, Bizien L, Trouillet-Assant S, Dobbs K, Jesus AA de, Belot A, Kallaste A, Catherinot E, Tandjaoui-Lambiotte Y, Pen JL, Kerner G, Bigio B, Seeleuthner Y, Yang R, Bolze A, Spaan AN, Delmonte OM, Abers MS, Aiuti A, Casari G, Lampasona V, Piemonti L, Ciceri F, Bilguvar K, Lifton RP, Vasse M, Smadja DM, Migaud M, Hadjadj J, Terrier B, Duffy D, Quintana-Murci L, Beek D van de, Roussel L, Vinh DC, Tangye SG, Haerynck F, Dalmau D, Martinez-Picado J, Brodin P, Nussenzweig MC, Boisson-Dupuis S, Rodríguez-Gallego C, Vogt G, Mogensen TH, Oler AJ, Gu J, Burbelo PD, Cohen J, Biondi A, Bettini LR, D'Angio M, Bonfanti P, Rossignol P, Mayaux J, Rieux-Laucat F, Husebye ES, Fusco F, Ursini MV, Imberti L, Sottini A, Paghera S, Quiros-Roldan E, Rossi C, Castagnoli R, Montagna D, Licari A, Marseglia GL, Duval X, Ghosn J, Lab§ H, Group§ N-UIR to C, Clinicians§ C, Clinicians§ C-S, Group§ IC, Group§ FCCS, Consortium§ TMI, Cohort§ C-C, Biobank§ AUC-19, Effort§ CHG, Tsang JS, Goldbach-Mansky R, Kisand K, Lionakis MS, Puel A, Zhang S-Y, Holland SM, Gorochov G, Jouanguy E, Rice CM, Cobat A, Notarangelo LD, Abel L, Su HC,

Casanova J-L. 2020. Auto-antibodies against type I IFNs in patients with life-threatening COVID-19. *Science* eabd4585. doi:10.1126/science.abd4585

Blanco-Melo D, Nilsson-Payant BE, Liu W-C, Uhl S, Hoagland D, Møller R, Jordan TX, Oishi K, Panis M, Sachs D, Wang TT, Schwartz RE, Lim JK, Albrecht RA, tenOever BR. 2020. Imbalanced Host Response to SARS-CoV-2 Drives Development of COVID-19. *Cell* 181:1036-1045.e9. doi:10.1016/j.cell.2020.04.026

Boada-Romero E, Martinez J, Heckmann B, Green D. 2020. The clearance of dead cells by efferocytosis. *Nat Rev Mol Cell Bio* 1–17. doi:10.1038/s41580-020-0232-1

Bosurgi L, Cao YG, Cabeza-Cabrerizo M, Tucci A, Hughes LD, Kong Y, Weinstein JS, Licona-Limon P, Schmid ET, Pelorosso F, Gagliani N, Craft JE, Flavell RA, Ghosh S, Rothlin CV. 2017. Macrophage function in tissue repair and remodeling requires IL-4 or IL-13 with apoptotic cells. *Sci New York N Y* 356:1072–1076. doi:10.1126/science.aai8132

Chan JF-W, Zhang AJ, Yuan S, Poon VK-M, Chan CC-S, Lee AC-Y, Chan W-M, Fan Z, Tsoi H-W, Wen L, Liang R, Cao J, Chen Y, Tang K, Luo C, Cai J-P, Kok K-H, Chu H, Chan K-H, Sridhar S, Chen Z, Chen H, To KK-W, Yuen K-Y. 2020. Simulation of the Clinical and Pathological Manifestations of Coronavirus Disease 2019 (COVID-19) in a Golden Syrian Hamster Model: Implications for Disease Pathogenesis and Transmissibility. *Clin Infect Dis Official Publ Infect Dis Soc Am* 71:2428–2446. doi:10.1093/cid/ciaa325

Chen L, Long X, Xu Q, Tan J, Wang G, Cao Y, Wei J, Luo H, Zhu H, Huang Liang, Meng F, Huang Lifang, Wang N, Zhou X, Zhao L, Chen X, Mao Z, Chen C, Li Z, Sun Z, Zhao J, Wang D, Huang G, Wang W, Zhou J. 2020. Elevated serum levels of S100A8/A9 and HMGB1 at hospital admission are correlated with inferior clinical outcomes in COVID-19 patients. *Cell Mol Immunol* 17:992–994. doi:10.1038/s41423-020-0492-x

Chu H, Chan JF-W, Yuen TT-T, Shuai H, Yuan S, Wang Y, Hu B, Yip CC-Y, Tsang JO-L, Huang X, Chai Y, Yang D, Hou Y, Chik KK-H, Zhang X, Fung AY-F, Tsoi H-W, Cai J-P, Chan W-M, Ip JD, Chu AW-H, Zhou J, Lung DC, Kok K-H, To KK-W, Tsang OT-Y, Chan K-H, Yuen K-Y. 2020. Comparative tropism, replication kinetics, and cell damage profiling of SARS-CoV-2 and SARS-CoV with implications for clinical manifestations, transmissibility, and laboratory studies of COVID-19: an observational study. *Lancet Microbe* 1:e14–e23. doi:10.1016/s2666-5247(20)30004-5

Chu H, Shuai H, Hou Y, Zhang X, Wen L, Huang X, Hu B, Yang D, Wang Y, Yoon C, Wong BH-Y, Li C, Zhao X, Poon VK-M, Cai J-P, Wong KK-Y, Yeung M-L, Zhou J, Au-Yeung RK-H, Yuan S, Jin D-Y, Kok K-H, Perlman S, Chan JF-W, Yuen K-Y. 2021. Targeting highly pathogenic coronavirus-induced apoptosis reduces viral pathogenesis and disease severity. *Sci Adv* 7:eabf8577. doi:10.1126/sciadv.abf8577

Corman VM, Landt O, Kaiser M, Molenkamp R, Meijer A, Chu DK, Bleicker T, Brünink S, Schneider J, Schmidt ML, Mulders DG, Haagmans BL, Veer B van der, Brink S van den, Wijsman L, Goderski G, Romette J-L, Ellis J, Zambon M, Peiris M, Goossens H, Reusken C, Koopmans MP, Drosten C. 2020. Detection of 2019 novel coronavirus (2019-nCoV) by real-time RT-PCR. *Eurosurveillance* 25:2000045. doi:10.2807/1560-7917.es.2020.25.3.2000045

Doran AC, Yurdagul A, Tabas I. 2020. Efferocytosis in health and disease. *Nat Rev Immunol* 20:254–267. doi:10.1038/s41577-019-0240-6

Evavold CL, Ruan J, Tan Y, Xia S, Wu H, Kagan JC. 2017. The Pore-Forming Protein Gasdermin D Regulates Interleukin-1 Secretion from Living Macrophages. Immunity 48:35-44.e6. doi:10.1016/j.immuni.2017.11.013

Fadok VA, Voelker DR, Campbell PA, Cohen JJ, Bratton DL, Henson PM. 1992. Exposure of phosphatidylserine on the surface of apoptotic lymphocytes triggers specific recognition and removal by macrophages. *J Immunol Baltim Md 1950* 148:2207–16.

Feng X, Deng T, Zhang Y, Su S, Wei C, Han D. 2011. Lipopolysaccharide inhibits macrophage phagocytosis of apoptotic neutrophils by regulating the production of tumour necrosis factor α and growth arrest-specific gene 6. *Immunology* 132:287–295. doi:10.1111/j.1365-2567.2010.03364.x

Frank A, Rauen U, Groot H de. 2000. Protection by glycine against hypoxic injury of rat hepatocytes: inhibition of ion fluxes through nonspecific leaks. J Hepatol 32:58–66. doi:10.1016/s0168-8278(00)80190-7

Gomes R, Guerra-Sá R, Arruda E. 2009. Coxsackievirus B5 induced apoptosis of HeLa cells: effects on p53 and SUMO. *Virology* 396:256–63. doi:10.1016/j.virol.2009.10.005

Hamers AAJ, Dinh HQ, Thomas GD, Marcovecchio P, Blatchley A, Nakao CS, Kim C, McSkimming C, Taylor AM, Nguyen AT, McNamara CA, Hedrick CC. 2019. Human Monocyte Heterogeneity as Revealed by High-Dimensional Mass Cytometry. *Arteriosclerosis Thrombosis Vasc Biology* 39:25–36. doi:10.1161/atvbaha.118.311022

Han Y, Zhang H, Mu S, Wei W, Jin C, Xue Y, Tong C, Zha Y, Song Z, Gu G. 2020. Lactate dehydrogenase, a Risk Factor of Severe COVID-19 Patients. *Medrxiv* 2020.03.24.20040162. doi:10.1101/2020.03.24.20040162

Jamieson AM, Pasman L, Yu S, Gamradt P, Homer RJ, Decker T, Medzhitov R. 2013. Role of Tissue Protection in Lethal Respiratory Viral-Bacterial Coinfection. *Science* 340:1230–1234. doi:10.1126/science.1233632

Korotkevich G, Sukhov V, Budin N, Shpak B, Artyomov MN, Sergushichev A. 2021. Fast gene set enrichment analysis. *Biorxiv* 060012. doi:10.1101/060012

Li Shaohua, Jiang L, Li X, Lin F, Wang Y, Li B, Jiang T, An W, Liu S, Liu H, Xu P, Zhao L, Zhang L, Mu J, Wang H, Kang J, Li Y, Huang L, Zhu C, Zhao S, Lu J, Ji J, Zhao J. 2020. Clinical and pathological investigation of patients with severe COVID-19. *Jci Insight* 5. doi:10.1172/jci.insight.138070

Li Shufen, Zhang Y, Guan Z, Li H, Ye M, Chen X, Shen J, Zhou Y, Shi Z-L, Zhou P, Peng K. 2020. SARS-CoV-2 triggers inflammatory responses and cell death through caspase-8 activation. *Signal Transduct Target Ther* 5:235. doi:10.1038/s41392-020-00334-0

Liao M, Liu Y, Yuan J, Wen Y, Xu G, Zhao J, Cheng L, Li J, Wang X, Wang F, Liu L, Amit I, Zhang S, Zhang Z. 2020. Single-cell landscape of bronchoalveolar immune cells in patients with COVID-19. *Nat Med* 26:842–844. doi:10.1038/s41591-020-0901-9

Lucas C, Wong P, Klein J, Castro TBR, Silva J, Sundaram M, Ellingson MK, Mao T, Oh JE, Israelow B, Takahashi T, Tokuyama M, Lu P, Venkataraman A, Park A, Mohanty S, Wang H, Wyllie AL, Vogels CBF, Earnest R, Lapidus S, Ott IM, Moore AJ, Muenker MC, Fournier JB, Campbell M, Odio CD, Casanovas-Massana A, Obaid A, Lu-Culligan A, Nelson A, Brito A, Nunez A, Martin A, Watkins A, Geng B, Kalinich C, Harden C, Todeasa C, Jensen C, Kim D, McDonald D, Shepard D, Courchaine E, White EB, Song E, Silva E, Kudo E, DeIuliis G, Rahming H, Park H-J, Matos I, Nouws J, Valdez J, Fauver J, Lim J, Rose K-A, Anastasio K, Brower K, Glick L, Sharma L, Sewanan L, Knaggs L, Minasyan M, Batsu M, Petrone M, Kuang M, Nakahata M, Campbell M, Linehan M, Askenase MH, Simonov M, Smolgovsky M, Sonnert N, Naushad N, Vijayakumar P, Martinello R, Datta R, Handoko R, Bermejo S, Prophet S, Bickerton S, Velazquez S, Alpert T, Rice T, Khoury-Hanold W, Peng X, Yang Y, Cao Y, Strong Y, Herbst R, Shaw AC, Medzhitov R, Schulz WL, Grubaugh ND, Cruz CD,

Farhadian S, Ko AI, Omer SB, Iwasaki A. 2020. Longitudinal analyses reveal immunological misfiring in severe COVID-19. *Nature* 584:463–469. doi:10.1038/s41586-020-2588-y

Martins R, Carlos AR, Braza F, Thompson JA, Bastos-Amador P, Ramos S, Soares MP. 2019. Disease Tolerance as an Inherent Component of Immunity. *Annu Rev Immunol* 37:405–437. doi:10.1146/annurev-immunol-042718-041739

Michlewska S, Dransfield I, Megson IL, Rossi AG. 2008. Macrophage phagocytosis of apoptotic neutrophils is critically regulated by the opposing actions of pro-inflammatory and anti-inflammatory agents: key role for TNF-alpha. *Faseb J Official Publ Fed Am Soc Exp Biology* 23:844–54. doi:10.1096/fj.08-121228

Miyanishi M, Tada K, Koike M, Uchiyama Y, Kitamura T, Nagata S. 2007. Identification of Tim4 as a phosphatidylserine receptor. *Nature* 450:435–439. doi:10.1038/nature06307

Morioka S, Perry JSA, Raymond MH, Medina CB, Zhu Y, Zhao L, Serbulea V, Onengut-Gumuscu S, Leitinger N, Kucenas S, Rathmell JC, Makowski L, Ravichandran KS. 2018. Efferocytosis induces a novel SLC program to promote glucose uptake and lactate release. *Nature* 563:714–718. doi:10.1038/s41586-018-0735-5

Mulay A, Konda B, Garcia G, Yao C, Beil S, Villalba JM, Koziol C, Sen C, Purkayastha A, Kolls JayK, Pociask DA, Pessina P, Aja JS de, Garcia-de-Alba C, Kim CF, Gomperts B, Arumugaswami V, Stripp BR. 2021. SARS-CoV-2 infection of primary human lung epithelium for COVID-19 modeling and drug discovery. *Cell Reports* 35:109055. doi:10.1016/j.celrep.2021.109055

Murray PJ, Wynn TA. 2011. Protective and pathogenic functions of macrophage subsets. *Nat Rev Immunol* 11:723–737. doi:10.1038/nri3073

Mylvaganam S, Freeman SA, Grinstein S. 2021. The cytoskeleton in phagocytosis and macropinocytosis. *Curr Biol* 31:R619–R632. doi:10.1016/j.cub.2021.01.036

Nagata S. 2018. Apoptosis and Clearance of Apoptotic Cells. *Annu Rev Immunol* 36:489–517. doi:10.1146/annurev-immunol-042617-053010

Olagnier D, Lavergne R-A, Meunier E, Lefèvre L, Dardenne C, Aubouy A, Benoit-Vical F, Ryffel B, Coste A, Berry A, Pipy B. 2011. Nrf2, a PPARγ Alternative Pathway to Promote CD36 Expression on Inflammatory Macrophages: Implication for Malaria. *Plos Pathog* 7:e1002254. doi:10.1371/journal.ppat.1002254

Park D, Han CZ, Elliott MR, Kinchen JM, Trampont PC, Das S, Collins S, Lysiak JJ, Hoehn KL, Ravichandran KS. 2011. Continued clearance of apoptotic cells critically depends on the phagocyte Ucp2 protein. *Nature* 477:220–4. doi:10.1038/nature10340

Parks BW, Black LL, Zimmerman KA, Metz AE, Steele C, Murphy-Ullrich JE, Kabarowski JH. 2013. CD36, but not G2A, modulates efferocytosis, inflammation, and fibrosis following bleomycin-induced lung injury[S]. *J Lipid Res* 54:1114–1123. doi:10.1194/jlr.m035352

Penberthy KK, Ravichandran KS. 2016. Apoptotic cell recognition receptors and scavenger receptors. *Immunological reviews* 269:44–59. doi:10.1111/imr.12376

Peng Y, Elkon KB. 2011. Autoimmunity in MFG-E8–deficient mice is associated with altered trafficking and enhanced cross-presentation of apoptotic cell antigens. *J Clin Invest* 121:2221–2241. doi:10.1172/jci43254

Perry JSA, Morioka S, Medina CB, Etchegaray JI, Barron B, Raymond MH, Lucas CD, Onengut-Gumuscu S, Delpire E, Ravichandran KS. 2019. Interpreting an apoptotic corpse as anti-inflammatory involves a chloride sensing pathway. *Nat Cell Biol* 21:1532–1543. doi:10.1038/s41556-019-0431-1

Reed LJ, Muench H. 1938. A simple method of estimating fifty per cent endpoints. *Am J Epidemiol* 27:493–497. doi:10.1093/oxfordjournals.aje.a118408

Ren X, Wen W, Fan X, Hou W, Su Bin, Cai P, Li J, Liu Y, Tang F, Zhang F, Yang Y, He Jiangping, Ma W, He Jingjing, Wang P, Cao Q, Chen F, Chen Y, Cheng X, Deng G, Deng X, Ding W, Feng Y, Gan R, Guo C, Guo W, He S, Jiang C, Liang J, Li Y, Lin J, Ling Y, Liu H, Liu J, Liu N, Liu S-Q, Luo M, Ma Q, Song Q, Sun W, Wang G, Wang F, Wang Y, Wen X, Wu Q, Xu G, Xie X, Xiong X, Xing X, Xu H, Yin C, Yu D, Yu K, Yuan J, Zhang B, Zhang P, Zhang T, Zhao J, Zhao Peidong, Zhou J, Zhou W, Zhong S, Zhong X, Zhang S, Zhu L, Zhu P, Zou B, Zou J, Zuo Z, Bai F, Huang X, Zhou P, Jiang Q, Huang Z, Bei J-X, Wei L, Bian X-W, Liu X, Cheng T, Li X, Zhao Pingsen, Wang F-S, Wang H, Su Bing, Zhang Zheng, Qu K, Wang X, Chen J, Jin R, Zhang Zemin. 2021. COVID-19 immune features revealed by a large-scale single-cell transcriptome atlas. *Cell* 184:1895-1913.e19. doi:10.1016/j.cell.2021.01.053

Ren Y, Shu T, Wu D, Mu J, Wang C, Huang M, Han Y, Zhang X-Y, Zhou W, Qiu Y, Zhou X. 2020. The ORF3a protein of SARS-CoV-2 induces apoptosis in cells. *Cell Mol Immunol* 17:881–883. doi:10.1038/s41423-020-0485-9

Rodrigues TS, Sá KSG de, Ishimoto AY, Becerra A, Oliveira S, Almeida L, Gonçalves AV, Perucello DB, Andrade WA, Castro R, Veras FP, Toller-Kawahisa JE, Nascimento DC, Lima MHF de, Silva CMS, Caetite DB, Martins RB, Castro IA, Pontelli MC, Barros FC de, Amaral NB do, Giannini MC, Bonjorno LP, Lopes MIF, Santana RC, Vilar FC, Auxiliadora-Martins M, Luppino-Assad R, Almeida SCL de, Oliveira FR de, Batah SS, Siyuan L, Benatti MN, Cunha TM, Alves-Filho JC, Cunha FQ, Cunha LD, Frantz FG, Kohlsdorf T, Fabro AT, Arruda E, Oliveira RDR de, Louzada-Junior P, Zamboni DS. 2020. Inflammasomes are activated in response to SARS-CoV-2 infection and are associated with COVID-19 severity in patients. *J Exp Med* 218. doi:10.1084/jem.20201707

Rodriguez-Manzanet R, Sanjuan MA, Wu HY, Quintana FJ, Xiao S, Anderson AC, Weiner HL, Green DR, Kuchroo VK. 2010. T and B cell hyperactivity and autoimmunity associated with niche-specific defects in apoptotic body clearance in TIM-4-deficient mice. *Proc National Acad Sci* 107:8706–8711. doi:10.1073/pnas.0910359107

Rothlin CV, Hille TD, Ghosh S. 2020. Determining the effector response to cell death. *Nat Rev Immunol* 1–13. doi:10.1038/s41577-020-00456-0

Satyanarayanan SK, Kebir DE, Soboh S, Butenko S, Sekheri M, Saadi J, Peled N, Assi S, Othman A, Schif-Zuck S, Feuermann Y, Barkan D, Sher N, Filep JG, Ariel A. 2019. IFN-β is a macrophage-derived effector cytokine facilitating the resolution of bacterial inflammation. *Nat Commun* 10:3471. doi:10.1038/s41467-019-10903-9

Schulte-Schrepping J, Reusch N, Paclik D, Baßler K, Schlickeiser S, Zhang B, Krämer B, Krammer T, Brumhard S, Bonaguro L, Domenico ED, Wendisch D, Grasshoff M, Kapellos TS, Beckstette M, Pecht T, Saglam A, Dietrich O, Mei HE, Schulz AR, Conrad C, Kunkel D, Vafadarnejad E, Xu C-J, Horne A, Herbert M, Drews A, Thibeault C, Pfeiffer M, Hippenstiel S, Hocke A, Müller-Redetzky H, Heim K-M, Machleidt F, Uhrig A, Jarcy LB de, Jürgens L, Stegemann M, Glösenkamp CR, Volk H-D, Goffinet C, Landthaler M, Wyler E, Georg P, Schneider M, Dang-Heine C, Neuwinger N, Kappert K, Tauber R, Corman V, Raabe J, Kaiser KM, Vinh MT, Rieke G, Meisel C, Ulas T, Becker M, Geffers R, Witzenrath M, Drosten C, Suttorp N, Kalle C von, Kurth F, Händler K, Schultze JL, Aschenbrenner AC, Li Y, Nattermann J, Sawitzki B, Saliba A-E, Sander LE, (DeCOI) DC-19 OI, Angelov A, Bals R, Bartholomäus A, Becker A, Bezdan D, Bonifacio E, Bork P, Clavel T, Colome-Tatche M, Diefenbach A, Dilthey A, Fischer N, Förstner K, Frick J-S, Gagneur J, Goesmann A, Hain T,

Hummel M, Janssen S, Kalinowski J, Kallies R, Kehr B, Keller A, Kim-Hellmuth S, Klein C, Kohlbacher O, Korbel JO, Kurth I, Landthaler M, Li Y, Ludwig K, Makarewicz O, Marz M, McHardy A, Mertes C, Nöthen M, Nürnberg P, Ohler U, Ossowski S, Overmann J, Peter S, Pfeffer K, Poetsch AR, Pühler A, Rajewsky N, Ralser M, Rieß O, Ripke S, Rocha UN da, Rosenstiel P, Saliba A-E, Sander LE, Sawitzki B, Schiffer P, Schulte E-C, Schultze JL, Sczyrba A, Stegle O, Stoye J, Theis F, Vehreschild J, Vogel J, Kleist M von, Walker A, Walter J, Wieczorek D, Ziebuhr J. 2020. Severe COVID-19 Is Marked by a Dysregulated Myeloid Cell Compartment. *Cell* 182:1419-1440.e23. doi:10.1016/j.cell.2020.08.001

Siddiqi HK, Mehra MR. 2020. COVID-19 Illness in Native and Immunosuppressed States: A Clinical-Therapeutic Staging Proposal. *J Hear Lung Transplant*. doi:10.1016/j.healun.2020.03.012

Silvin A, Chapuis N, Dunsmore G, Goubet A-G, Dubuisson A, Derosa L, Almire C, Hénon C, Kosmider O, Droin N, Rameau P, Catelain C, Alfaro A, Dussiau C, Friedrich C, Sourdeau E, Marin N, Szwebel T-A, Cantin D, Mouthon L, Borderie D, Deloger M, Bredel D, Mouraud S, Drubay D, Andrieu M, Lhonneur A-S, Saada V, Stoclin A, Willekens C, Pommeret F, Griscelli F, Ng LG, Zhang Z, Bost P, Amit I, Barlesi F, Marabelle A, Pène F, Gachot B, André F, Zitvogel L, Ginhoux F, Fontenay M, Solary E. 2020. Elevated Calprotectin and Abnormal Myeloid Cell Subsets Discriminate Severe from Mild COVID-19. *Cell* 182:1401-1418.e18. doi:10.1016/j.cell.2020.08.002

Tait JF, Smith C. 1999. Phosphatidylserine Receptors: Role of CD36 in Binding of Anionic Phospholipid Vesicles to Monocytic Cells*. *J Biol Chem* 274:3048–3054. doi:10.1074/jbc.274.5.3048

Thorp E, Vaisar T, Subramanian M, Mautner L, Blobel C, Tabas I. 2011. Shedding of the Mer Tyrosine Kinase Receptor Is Mediated by ADAM17 Protein through a Pathway Involving Reactive Oxygen Species, Protein Kinase Cδ, and p38 Mitogen-activated Protein Kinase (MAPK). *J Biol Chem* 286:33335–33344. doi:10.1074/jbc.m111.263020

Trzebanski S, Jung S. 2020. Plasticity of monocyte development and monocyte fates. *Immunol Lett* 227:66–78. doi:10.1016/j.imlet.2020.07.007

Valle DMD, Kim-Schulze S, Huang H-H, Beckmann ND, Nirenberg S, Wang B, Lavin Y, Swartz TH, Madduri D, Stock A, Marron TU, Xie H, Patel M, Tuballes K, Oekelen OV, Rahman A, Kovatch P, Aberg JA, Schadt E, Jagannath S, Mazumdar M, Charney AW, Firpo-Betancourt A, Mendu DR, Jhang J, Reich D, Sigel K, Cordon-Cardo C, Feldmann M, Parekh S, Merad M, Gnjatic S. 2020. An inflammatory cytokine signature predicts COVID-19 severity and survival. *Nat Med* 26:1636–1643. doi:10.1038/s41591-020-1051-9

Veras FP, Pontelli MC, Silva CM, Toller-Kawahisa JE, Lima M de, Nascimento DC, Schneider AH, Caetité D, Tavares LA, Paiva IM, Rosales R, Colón D, Martins R, Castro IA, Almeida GM, Lopes MIF, Benatti MN, Bonjorno LP, Giannini MC, Luppino-Assad R, Almeida SL, Vilar F, Santana R, Bollela VR, Auxiliadora-Martins M, Borges M, Miranda CH, Pazin-Filho A, Silva LLP da, Cunha L, Zamboni DS, Dal-Pizzol F, Leiria LO, Siyuan L, Batah S, Fabro A, Mauad T, Dolhnikoff M, Duarte-Neto A, Saldiva P, Cunha TM, Alves-Filho JC, Arruda E, Louzada-Junior P, Oliveira RD, Cunha FQ. 2020. SARS-CoV-2–triggered neutrophil extracellular traps mediate COVID-19 pathology. *J Exp Med* 217. doi:10.1084/jem.20201129

Wang Y, Subramanian M, Yurdagul A, Barbosa-Lorenzi VC, Cai B, Juan-Sanz J de, Ryan TA, Nomura M, Maxfield FR, Tabas I. 2017. Mitochondrial Fission Promotes the Continued Clearance of Apoptotic Cells by Macrophages. *Cell* 171:331-345.e22. doi:10.1016/j.cell.2017.08.041

Webb BJ, Peltan ID, Jensen P, Hoda D, Hunter B, Silver A, Starr N, Buckel W, Grisel N, Hummel E, Snow G, Morris D, Stenehjem E, Srivastava R, Brown SM. 2020. Clinical criteria for COVID-19-associated hyperinflammatory syndrome: a cohort study. *Lancet Rheumatology*. doi:10.1016/s2665-9913(20)30343-x

Wu T, Hu E, Xu S, Chen M, Guo P, Dai Z, Feng T, Zhou L, Tang W, Zhan L, Fu X, Liu S, Bo X, Yu G. 2021. clusterProfiler 4.0: A universal enrichment tool for interpreting omics data. *Innovation* 2:100141. doi:10.1016/j.xinn.2021.100141

Yurdagul A, Subramanian M, Wang X, Crown SB, Ilkayeva OR, Darville L, Kolluru GK, Rymond CC, Gerlach BD, Zheng Z, Kuriakose G, Kevil CG, Koomen JM, Cleveland JL, Muoio DM, Tabas I. 2020. Macrophage Metabolism of Apoptotic Cell-Derived Arginine Promotes Continual Efferocytosis and Resolution of Injury. *Cell Metab* 31:518-533.e10. doi:10.1016/j.cmet.2020.01.001

Zhu N, Wang Wenling, Liu Z, Liang C, Wang Wen, Ye F, Huang B, Zhao L, Wang H, Zhou W, Deng Y, Mao L, Su C, Qiang G, Jiang T, Zhao J, Wu G, Song J, Tan W. 2020. Morphogenesis and cytopathic effect of SARS-CoV-2 infection in human airway epithelial cells. *Nat Commun* 11:3910. doi:10.1038/s41467-020-17796-z

Zuniga M, Gomes C, Carsons SE, Bender MT, Cotzia P, Miao QR, Lee DC, Rodriguez A. 2021. Autoimmunity to Annexin A2 predicts mortality among hospitalised COVID-19 patients. *Eur Respir J* 2100918. doi:10.1183/13993003.00918-2021

Zuo Y, Estes SK, Ali RA, Gandhi AA, Yalavarthi S, Shi H, Sule G, Gockman K, Madison JA, Zuo M, Yadav V, Wang J, Woodard W, Lezak SP, Lugogo NL, Smith SA, Morrissey JH, Kanthi Y, Knight JS. 2020. Prothrombotic autoantibodies in serum from patients hospitalized with COVID-19. *Sci Transl Med* 12:eabd3876. doi:10.1126/scitranslmed.abd3876

Figure captions

Figure 1. Macrophages engulf apoptotic cells carrying viable SARS-CoV-2

(A) Immunoblot of caspase-8 and caspase-3 cleavage in Calu-3 and Vero CCL81 cells in response to infection with SARS-CoV-2 for 48 h (CoV2, detected with rabbit anti-Spike), UV irradiation (UV) or freezing and thawing (F/T).

(B) Flow cytometric analysis of caspase-3 cleavage (Cl-caspase-3) in Calu-3 cells unstimulated (Cntrl) or infected with CoV2 for 48 h. The pan-caspase inhibitor z-VAD-FMK (zVAD; 20 μM) or vehicle (DMSO) were added to cell cultures after viral adsorption. Representative histogram, geometric mean fluorescence intensity (MFI), and frequency of Cl-caspase-3^+ cells (gated on Total

cells/Single cells) are shown. The black line on the histogram represents the control sample labeled with secondary antibody only.

(C) Flow cytometric analysis of apoptosis in Vero CCL81 cells in response to UV light irradiation or 48 h post-infection with CoV2, assessed by annexin V (FITC) and viability dye (Zombie NIR) co-staining. Representative histogram and frequency of each population (pre-gated on Total cells/Single cells) are shown.

(D) Cytotoxicity analysis by measurement of lactate dehydrogenase (LDH) release on the supernatants of Vero CCL81 cells in response to UV light irradiation or 48 h post-infection with CoV2.

(E, F) Representative histological findings in post-mortem lung tissue from COVID-19 patients obtained by ultrasound-guided minimally invasive autopsy. **(E)** Immunofluorescence images of tissue samples labeled with anti-Cl-caspase-3 (red), anti-dsRNA (green), and stained with Hoechst (nuclei, blue) for the detection of caspase-3 activation in infected epithelia (COVID-19, bottom panels) compared to samples from control patients (Cntrl, upper panels). Tissues were scanned by wide-field epifluorescence imaging. Scale bar: 20 μm, asterisks: erythrocytes. The mean fluorescence intensity (MFI) of Cl-caspase-3 of at least 300 cells are shown (n = 3 individuals per group). Technical control for secondary antibodies background is shown in Figure S1A. **(F)** Representative immunofluorescence image of a COVID-19 patient tissue sample labeled for the detection of efferocytosis in situ and superimposed with differential interference contrast. Samples were labeled with anti-CD68 (detecting macrophages, green), anti-cytokeratin18 (CK-18, detecting epithelial cells, white), anti-Spike (detecting SARS-CoV-2, red), and stained with Hoechst (nuclei, blue). Bottom panels show higher magnification of (a, b) $CD68^{+}$ macrophage with CK-18 and Spike labeling in the cytosol and (c) $CD68^{+}$ only macrophage. White arrows: CK-

18$^+$ cells; asterisks: erythrocytes. Tissues were scanned by wide-field epifluorescence imaging. Scale bar: 20 μm; scale bar for insets: 10 μm.

(G) Quantification by $TCID_{50}$ of SARS-CoV-2 viral loads in Vero CCL81 cells infected for 48 h. Viral loads were estimated for pre-sorted (Total cells) or annexin V$^+$ (Ann$^+$ cells) cells isolated by magnetic separation.

(H) Uptake of apoptotic Vero CCL81 cells (labeled with CTFR) in response to UV irradiation (UV-AC) or infection with SARS-CoV-2 for 48 h (Cov2-AC) by human monocyte-derived macrophages (labeled with CTV). Macrophages were co-incubated with AC for 2 h, and internalization was assessed by flow cytometry. Representative plot and percentage of engulfment (gated on Total cells/Single cells/Live cells/CTV$^+$/ CTV$^+$CTFR$^+$ cells) are shown.

Boxes represent the mean of five (B, D), four (C, H), or three (G) biological replicates, and error bars are ± S.E.M. Each biological replicate is shown as a circle. Significance was calculated by ANOVA (B-D), Mann-Whitney test (E) or Student's test (G, H). *, $p<0.05$, **, $p<0.001$, ***, $p<0.0001$, comparing the indicated groups. Data shown are from one representative out of two (A, C, G) or three (B, D, H) experiments performed independently with similar results.

Figure 1 – figure supplement 1. Support data for Figure 1.

(A). Immunofluorescence images of tissue samples immunolabeled with secondary antibodies-only used for detection anti-cleaved Caspase-3 (red, anti-rabbit IgG conjugated to Alexa 594), anti-dsRNA (green, donkey anti-mouse IgG F(ab)′$_2$-Alexa 488), and stained with Hoechst (nuclei, blue) in Figure 1E. Tissues were scanned by wide-field epifluorescence imaging. Scale bar: 20 μm, asterisks: erythrocytes.

(B) $TCID_{50}$ quantification of SARS-CoV-2 viral loads from detached, apoptotic Calu-3 and Vero CCL81 cells (CoV2-AC, 1.0 x 10^6 cells) and their cell-free supernatants, collected 48 h post-infection and isolated as described in the Methods.

(C) Uptake of apoptotic Calu-3 and Vero CCL81 cells (labeled with CFSE) in response to UV irradiation (UV-AC) or infection with SARS-CoV-2 for 48 h (Cov2-AC) by THP-1-derived macrophages (labeled with CTFR). Macrophages were co-incubated with AC for 2 h, and internalization was assessed by flow cytometry. Representative gating strategy, plots, and percentage of engulfment (gated on Total cells/Single cells/Live cells/$CTFR^+$/$CTFR^+$ $CFSE^+$ cells) are shown.

(D) Representative maximal projection of scanning confocal images showing the uptake of UV-AC or CoV2-AC (from Vero CCL81 cells, CFSE-labeled, green) by human monocyte-derived macrophages after 2 h of co-incubation. Samples were stained with Hoechst (nuclei, blue) and were immunolabeled with anti-Spike (SARS-CoV-2, red) and anti-CD11b (macrophage, white). Scale bar: 5 μm.

(E) Human monocyte-derived macrophages or THP-1-derived macrophages were unstimulated (Cntrl), co-incubated with apoptotic Vero CCL81 cells isolated from UV-irradiated (UV-AC) or SARS-CoV-2-infected (CoV2-AC) cultures, stimulated with the supernatants of infected apoptotic cells (CoV2-AC Sup), or infected with SARS-CoV-2 (CoV2), as indicated. The percentage of cellular viability was measured using a viability probe 24 h post-stimulation and analysis by flow cytometry (gated on Total cells/Single cells).

Boxes represent the mean of three biological replicates, and error bars are ± S.E.M. Each biological replicate is shown as a circle. Significance was calculated by Student's test (B-C) or ANOVA (E). *, $p<0.05$, **, $p<0.001$, ***, $p<0.0001$, comparing the indicated groups; ns: non-significant. Data

995 shown are from one representative out of two (B, C) or three (E) experiments performed
996 independently with similar results.
997
998 **Figure. 2. Engulfment of SARS-CoV-2-infected dying cells impairs macrophage anti-**
999 **inflammatory functions.**
1000 Macrophages were unstimulated (Cntrl), co-incubated with apoptotic Vero CCL81 cells (AC)
1001 isolated from UV-irradiated (UV-AC) or SARS-CoV-2-infected (CoV2-AC) cultures, stimulated
1002 with the supernatants of infected apoptotic cells (CoV2-AC Sup), or infected with CoV2 (CoV2),
1003 as indicated.
1004 **(A)** Heatmap showing the expression of M2-marker genes (*CCL18*, *MRC1*, *MMP9*, *PPARG,* and
1005 *CD163*) in human monocyte-derived macrophages 24 h after stimulation, calculated as $\log_2$ fold
1006 change relative to Cntrl. mRNA expression was determined by RT-qPCR and normalized to
1007 *GAPDH*. Data represent the mean of biological triplicates.
1008 **(B)** Flow cytometric analysis of CD206 expression on the cell surface of human monocyte-derived
1009 macrophages (gated on Total cells/Single cells/Live cells; gating strategy in Figure 2 – figure
1010 supplement 1A) 24 h after stimulation. Representative histograms and quantification of geometric
1011 mean fluorescence intensity (MFI) are shown. The black line on the histogram represents FMO
1012 control.
1013 **(C-E)** Flow cytometric analysis of CD206 expression on the cell surface of THP1-derived
1014 macrophages 24 h after stimulation, showing quantification of CD206 MFI. **(C)** Macrophages
1015 (labeled with CTFR) were stimulated with UV-AC or CoV2-AC (labeled with CTV) and CD206
1016 expression was measured on macrophages that engulfed (+) or not (-) AC. Gating strategy is
1017 depicted in Figure 2- figure supplement 1E. **(D)** Where indicated, isolated CoV2-AC were UV-

irradiated for 20 min prior to co-incubation for viral inactivation. **(E)** The responses of macrophages to UV-AC and CoV2-AC were compared to infection with CoV2 in the presence of UV-AC (UV-AC + CoV2).

Boxes represent the mean of three biological replicates using cells from a single donor (A, B) or THP-1-derived cells (C-E), and error bars are ± S.E.M. Each biological replicate is shown as a circle. Significance was calculated by ANOVA. *, $p<0.05$, **, $p<0.001$, ***, $p<0.0001$, comparing the indicated groups. Data shown are from one representative out of at least two experiments performed independently with similar results.

Figure 2 – figure supplement 1. Support data for Figure 2.

(A) Representative gating strategy used to determine the CD206 expression on the surface of macrophages in response to the different stimulus by flow cytometry (backgating corresponds to FMO control showed in Figure 2B).

(B) THP-1-derived macrophages were unstimulated (Cntrl), co-incubated with UV-AC, CoV2-AC, or CoV2-AC Sup obtained from Vero CCL81 cells, or infected with CoV2, as indicated. Expression of *MRC1* in macrophages showed as fold change relative to Cntrl was assessed 24 h after stimulation. mRNA expression was determined by RT-qPCR and normalized to *GAPDH*.

(C-D) THP-1-derived macrophages were incubated with UV-AC, Cov2-AC, or CoV2-Sup obtained from **(C)** Calu-3 or **(D)** Vero CCL81 infected cell cultures. CD206 expression on the cell surface 24h after stimulation was assessed by flow cytometry (gated on Total cells/Single cells/Live cells). Representative histograms and quantification of geometric mean fluorescence intensity (MFI) of CD206 are shown.

(E) Representative gating strategy used to determine the CD206 expression on the surface of CTFR-labeled macrophages stimulated with CTV-labeled AC in Figure 2C.

(F) Quantification by $TCID_{50}$ of the SARS-CoV-2 viral loads in 1.0×10^6 AC isolated from Vero CCL81 infected cells, either intact (CoV2-AC) or UV-irradiated for 20 min for viral inactivation (CoV2-AC UV).

Boxes represent the mean of three biological replicates, and error bars are ± S.E.M. Each biological replicate is shown as a circle. Significance was calculated by ANOVA (B-D) *, $p<0.05$, **, $p<0.001$, ***, $p<0.0001$, comparing the indicated groups; ns: non-significant. Data shown are from one representative out of two experiments performed independently with similar results.

Figure. 3. Engulfment of SARS-CoV-2-infected dying cells causes inflammatory cytokine production

Macrophages were unstimulated (Cntrl), co-incubated with apoptotic Vero CCL81 cells (AC) isolated from UV-irradiated (UV-AC) or SARS-CoV-2-infected (CoV2-AC) cultures, stimulated with the supernatants of infected apoptotic cells (CoV2-AC Sup), or infected with CoV2, as indicated.

(A) *IL6* expression in primary human monocyte-derived macrophages 24 h after stimulation showed as fold change relative to Cntrl. mRNA expression was determined by RT-qPCR and normalized to GAPDH.

(B) CBA quantification of IL-6 and IL-1β in the culture supernatants of the monocyte-derived macrophages 24 h after stimulation.

(C, D) ELISA quantification of IL-6 in the culture supernatants of THP1-derived macrophages 24 h after stimulation. **(C)** Macrophages were stimulated with early apoptotic AC (Annexin V^+

Zombie$^-$) or late apoptotic AC (Annexin V$^+$ Zombie$^+$) sorted out by flow cytometry. **(D)** Where indicated, isolated CoV2-AC were UV-irradiated (UV) for 20 min or fixed with 2% paraformaldehyde (Fix) for 10 min prior to co-incubation.

(E-H) ELISA quantification of IL-6 in the culture supernatants of human primary monocyte-derived macrophages 24 h after stimulation. **(E)** IL-6 secretion in response to CoV2-AC was compared to apoptotic cells isolated from Vero CCL81 cells similarly infected with Coxsackievirus (Coxsackie-AC). **(F)** PtdSer on the surface of CoV2-AC was blocked by incubation with Annexin V (Ann, 0.1 μg/mL) prior to addition to macrophage cultures to inhibit AC binding. **(G)** CoV2-AC and macrophages were co-incubated in the presence of Cytochalasin D (Cyto D, 10 μM) to inhibit AC internalization. **(H)** Macrophages were treated with Remdesivir (Remd, 20 μM) following stimulation with CoV2-AC to inhibit viral RNA transcription.

Boxes represent the mean of three biological replicates using cells from a single donor (A, B, F, G), two donors (E), or THP-1-derived cells (C, D), and error bars are ± S.E.M. Each biological replicate is shown as a circle. Significance was calculated by ANOVA. *, $p<0.05$, **, $p<0.001$, ***, $p<0.0001$, comparing the indicated groups. Data shown are from one representative out of at least two experiments performed independently with similar results.

Figure 3 – figure supplement 1. Support data for Figure 3.

(A) THP-1-derived macrophages were incubated with UV-AC, Cov2-AC, or CoV2-Sup obtained from infected Vero CCL81 cells or infected with CoV2. Expression of *IL6* in macrophages showed as fold change relative to Cntrl was assessed 24h after stimulation. mRNA expression was determined by RT-qPCR and normalized to *GAPDH*.

(B-C) THP-1-derived macrophages were incubated for 24 h with UV-AC, Cov2-C, or CoV2-Sup obtained from Calu-3 or Vero CCL81 infected cell cultures, as indicated. **(B)** IL-6 and **(C)** IL-1β in the culture supernatants were quantified by CBA.

(D) ELISA quantification of IL-6 in the culture supernatants of THP-1-derived macrophages incubated with UV-AC obtained from Vero CCL81 cells infected in the presence of glycine (Gly, 5 mM), where indicated, to inhibit release of cytosolic content due to permeabilization.

(E) Quantification by $TCID_{50}$ of the viral loads in 1.0 x 10^6 AC isolated from Vero CCL81 cells similarly infected with either Coxsackie virus (Coxsackie-AC) or SARS-CoV-2 (CoV2-AC).

(F) ELISA quantification of IL-6 in the culture supernatants of THP-1-derived macrophages stimulated with Cov2-AC for 24 h. PtdSer on the cell surface was blocked to inhibit AC binding by incubation of CoV2-AC with Annexin V (Ann, 0.01 and 0.1 μg/mL) prior to addition to macrophage cultures.

Boxes represent the mean of three (A, B, C, F) or four (D, E) biological replicates, and error bars are ± S.E.M. Each biological replicate is shown as a circle. Significance was calculated by ANOVA (A-D, F) or Student's test (E), *, $p<0.05$, **, $p<0.001$, ***, $p<0.0001$, comparing the indicated groups; ns: non-significant. Data shown are from one representative out of two experiments performed independently with similar results.

Figure 4. Engulfment of SARS-CoV-2-infected dying cells suppresses continual efferocytosis by macrophages

(**A**) Expression of efferocytic receptors in human primary monocyte-derived macrophages. Macrophages were unstimulated (Cntrl), co-incubated for 24 h with apoptotic Vero CCL81 cells (AC) isolated from UV-irradiated (UV-AC) or SARS-CoV-2-infected (CoV2-AC) cultures, or

infected with CoV2 (CoV2), as indicated. Expression of *CD36*, *SRA1*, *ITGB5*, *TIMD4*, and *MERTK* are showed as fold change relative to Cntrl. mRNA levels were determined by RT-qPCR and normalized to *GAPDH*.

(B-F) Flow cytometric analysis of two-step efferocytosis *in vitro*. THP-1-derived macrophages (CTV-labeled) were incubated with UV-AC or CoV2-AC isolated from Vero CCL81 cell cultures (labeled with pHRodo) for 18 h, and subsequently incubated with UV-irradiated apoptotic Jurkat cells (UV-Jurkat, CTFR-labeled) for 2 h. **(B)** Schematic representation of consecutive co-incubations of THP-1-derived macrophages with apoptotic cells prior to the assessment of cell corpse uptake by flow cytometry. **(C)** Representative maximal projection of scanning confocal images showing the uptake of AC (pHRodo) and UV-Jurkat (CTFR) by macrophages (CTV) after consecutive co-incubations. **(D)** Percentage of macrophages with internalized UV-AC or CoV2-AC (gated on Total cells/Single cells/Live cells/CTV^+/CTV^+ $pHRodo^+$); gating strategy is displayed in Figure 4- figure supplement 1B). **(E)** Percentage of macrophages that engulfed UV-Jurkat within $pHRodo^+$ populations (gated on Total cells/Single cells/Live cells/ CTV^+/$pHRodo^+$/ $pHRodo^+$ $CTFR^+$). **(F)** Percentage of macrophages that engulfed UV-Jurkat within $pHRodo^+$ populations (gates as in (E)) wherein macrophages were treated with Remdesivir (Remd, 20 μM) following stimulation with CoV2-AC.

Boxes represent the mean of three (A) or four (D-F) biological replicates using cells from a single donor in (A) or THP-1-derived macrophages (D-F), and error bars are ± S.E.M. Each biological replicate is shown as a circle. Significance was calculated by ANOVA (A, F) or Student's test (D, E). *, $p<0.05$, **, $p<0.001$, ***, $p<0.0001$, comparing the indicated groups. Data shown are from one representative out of three experiments performed independently with similar results.

Figure 4 – figure supplement 1. Support data for Figure 4.

(A) THP-1-derived macrophages were incubated with UV-AC or CoV2-AC obtained from infected Vero CCL81 cells or infected with CoV2. Expression of the efferocytic receptors *CD36*, *SRA-I*, *ITGB5*, *TIMD4*, and *MERTK* showed as fold change relative to Cntrl was assessed 24 h after stimulation. mRNA levels were determined by RT-qPCR and normalized to *GAPDH*.

(B) Representative gating strategy used to determine CTV-labeled macrophage populations for the two-step efferocytosis experiment showed in Figures 4D and E.

(C) THP-1-derived macrophages (CTV-labeled) were infected or not with SARS-CoV-2 (CoV2) for 18 h and subsequently were incubated with CTFR-labeled, UV-irradiated apoptotic Jurkat cells (UV-Jurkat) for 2 h. UV-Jurkat uptake is shown as the percentage of $CTFR^+$ (gated on Total cells/Single cells/Live cells/ CTV^+/ CTV^+ $CTFR^+$).

Boxes represent the mean of three biological replicates, and error bars are ± S.E.M. Each biological replicate is shown as a circle. Significance was calculated by ANOVA (A) or Student's test (C). *, $p<0.05$, **, $p<0.001$, ***, $p<0.0001$ comparing the indicated groups; ns: non-significant. Data shown are from one representative out of at least two experiments performed independently with similar results.

Figures 5. Lung monocytes and macrophages of severe COVID-19 patients express reduced levels of efferocytic receptors.

(A-B) Representative histological findings in post-mortem lung tissue from control patients (Cntrl) and COVID-19 patients, obtained by ultrasound-guided minimally invasive autopsy. Tissue samples were immunolabeled with anti-S100A9 (phagocytes, green), **(A)** anti-CD36 (red), or **(B)** anti-MERTK (red) and stained with DAPI (nuclei, blue). Representative images show cropped

details of lung tissues scanned by wide-field epifluorescence imaging. Scale bar: 10 µm. The mean fluorescence intensity (MFI) of CD36 and MERTK of at least 300 $S1009^+$ cells are shown (n = 6 control and 4 COVID-19 patient samples). Dots represent an $S1009^+$ cell (A and B), the crossing line represents the mean, and error bars are ± S.E.M. Significance was calculated by Mann-Whitney test (A and B), *, $p<0.05$, **, $p<0.001$, ***, $p<0.0001$, comparing the indicated groups. **(C)** GSEA analysis for efferocytosis-related gene sets in early-infiltrating phagocytes ($S1009^+$ $CCL18^-$) and in anti-inflammatory monocytes-derived macrophages ($CD14^+$ $S11009^-$ $CCL18^+$) clusters from the bronchoalveolar lavage of mild (M) and severe (S) COVID-19 patients versus healthy individuals. The corrplot depicts the normalized enrichment score (NES), and p value for the gene sets indicated on the y axis.

(D) Enriched efferocytosis-related Gene Ontology (GO) terms in genes repressed in virus-positive versus virus-negative alveolar macrophages.

Supplementary File 1. Custom gene sets incorporating associated to efferocytic pathway and related to human diseases (related to Figure 5C).

Supplementary File 2. Medical characteristics of COVID-19 patients.

Figure 1 **Salina, dos Santos, Rodrigues *et al.***

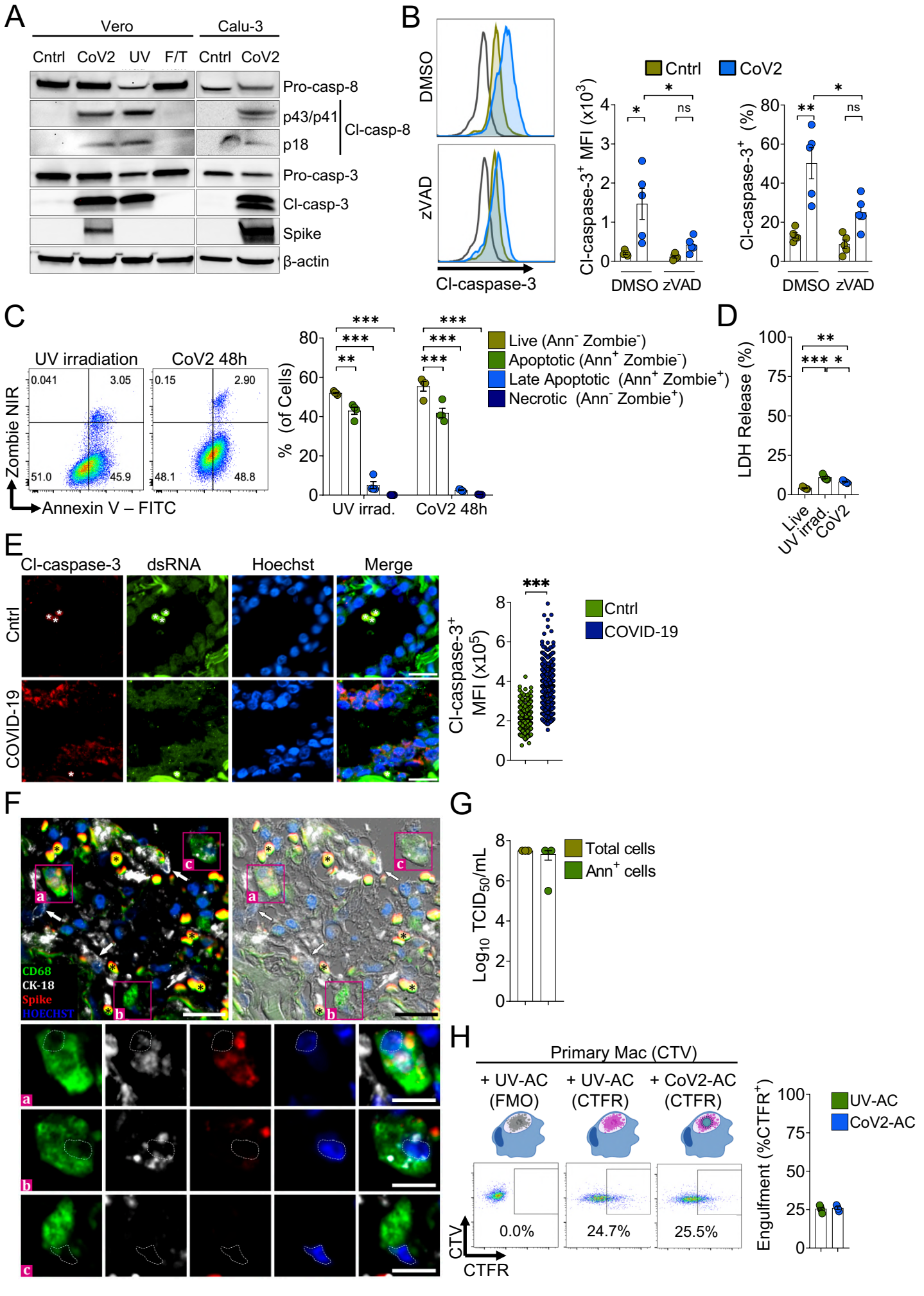

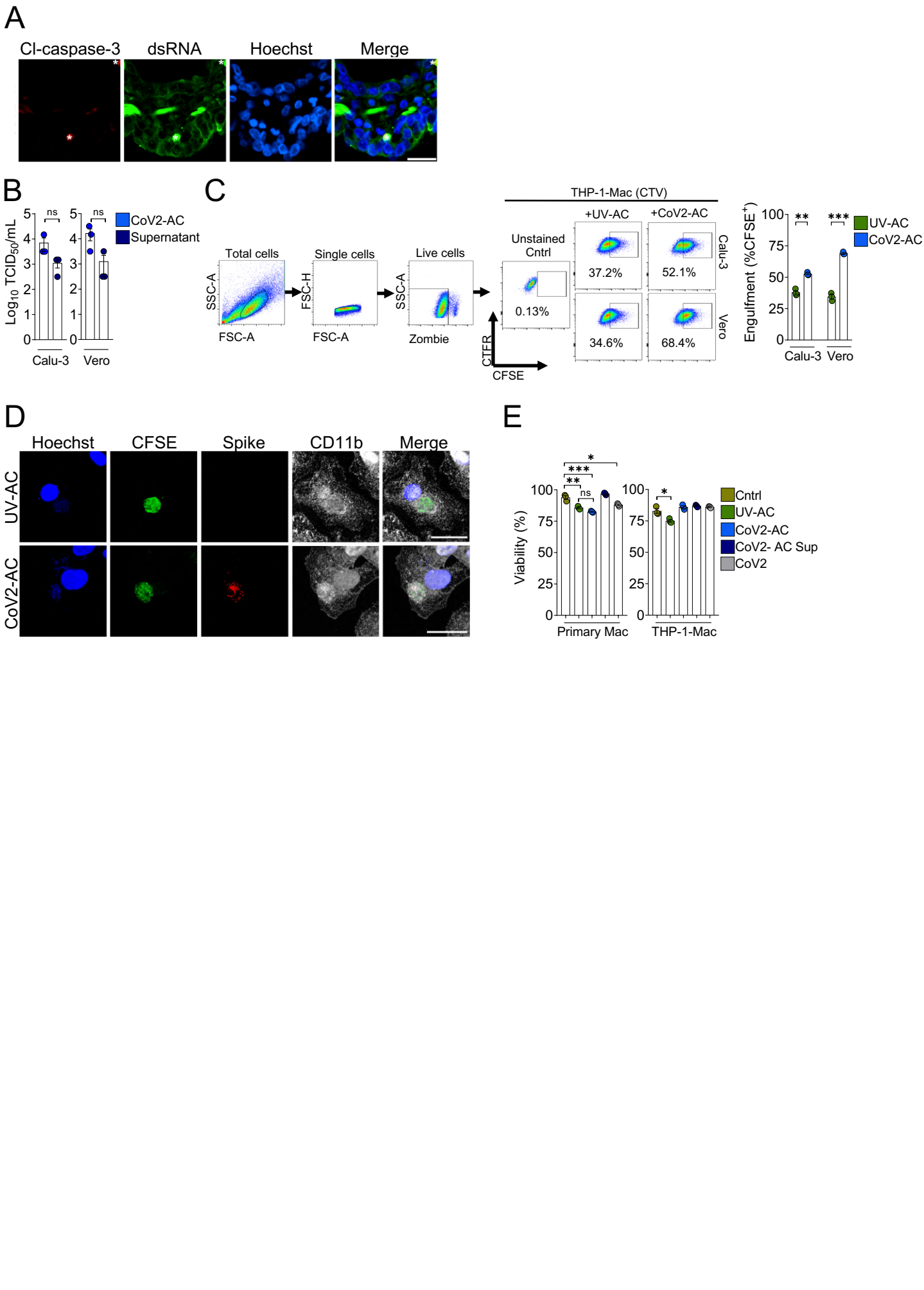

Figure 2 **Salina, dos Santos, Rodrigues *et al.***

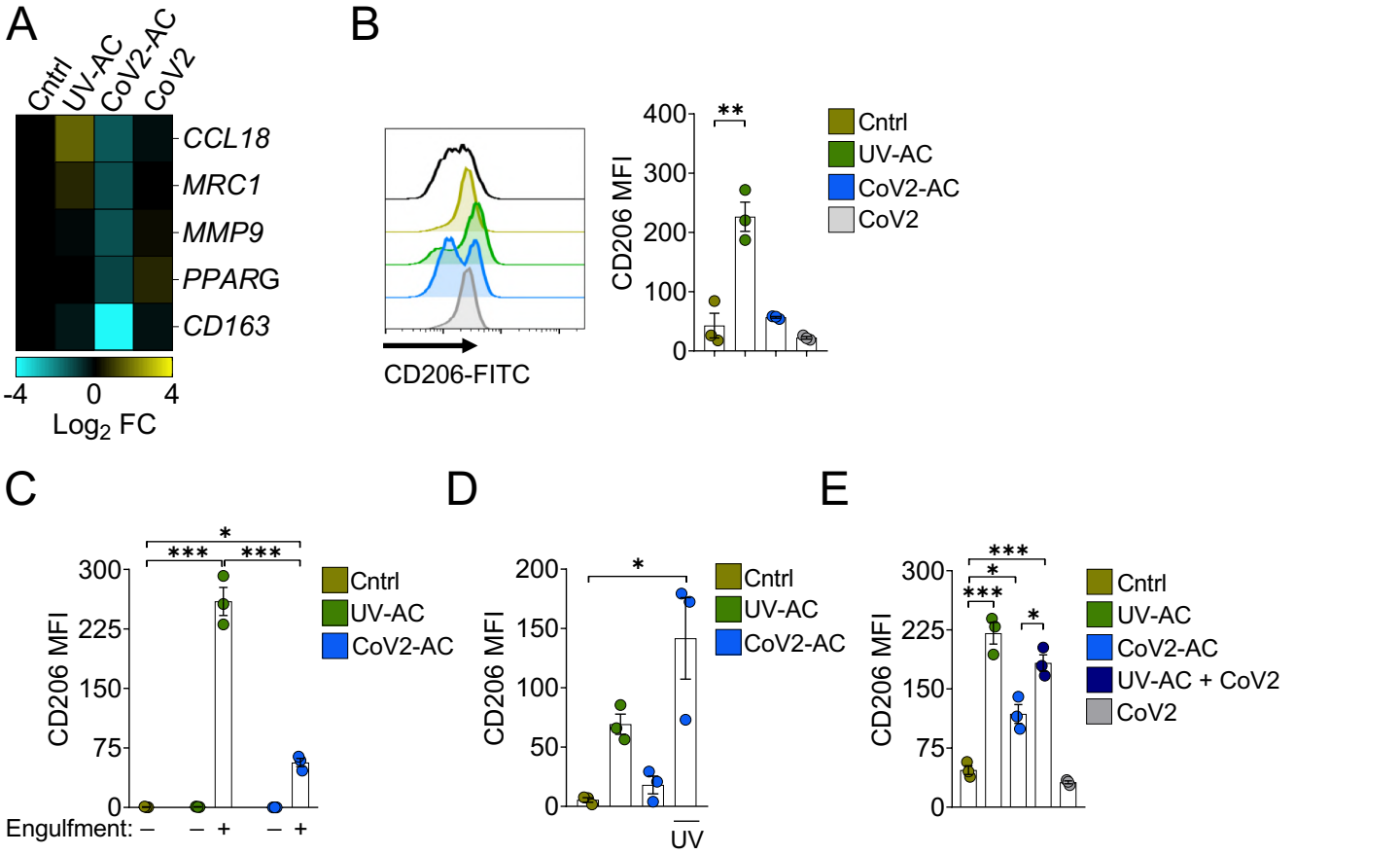

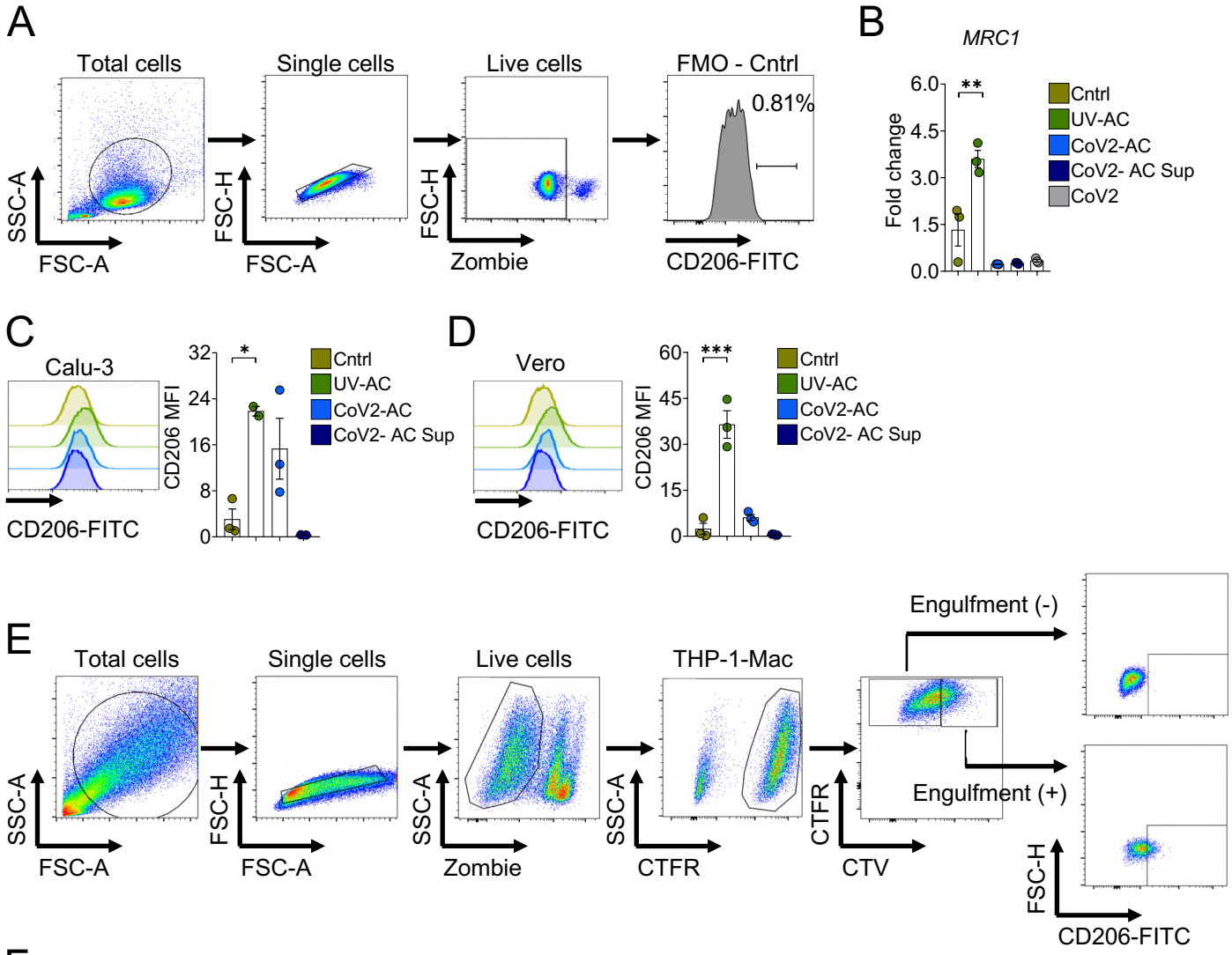

Figure 3 **Salina, dos Santos, Rodrigues *et al.***

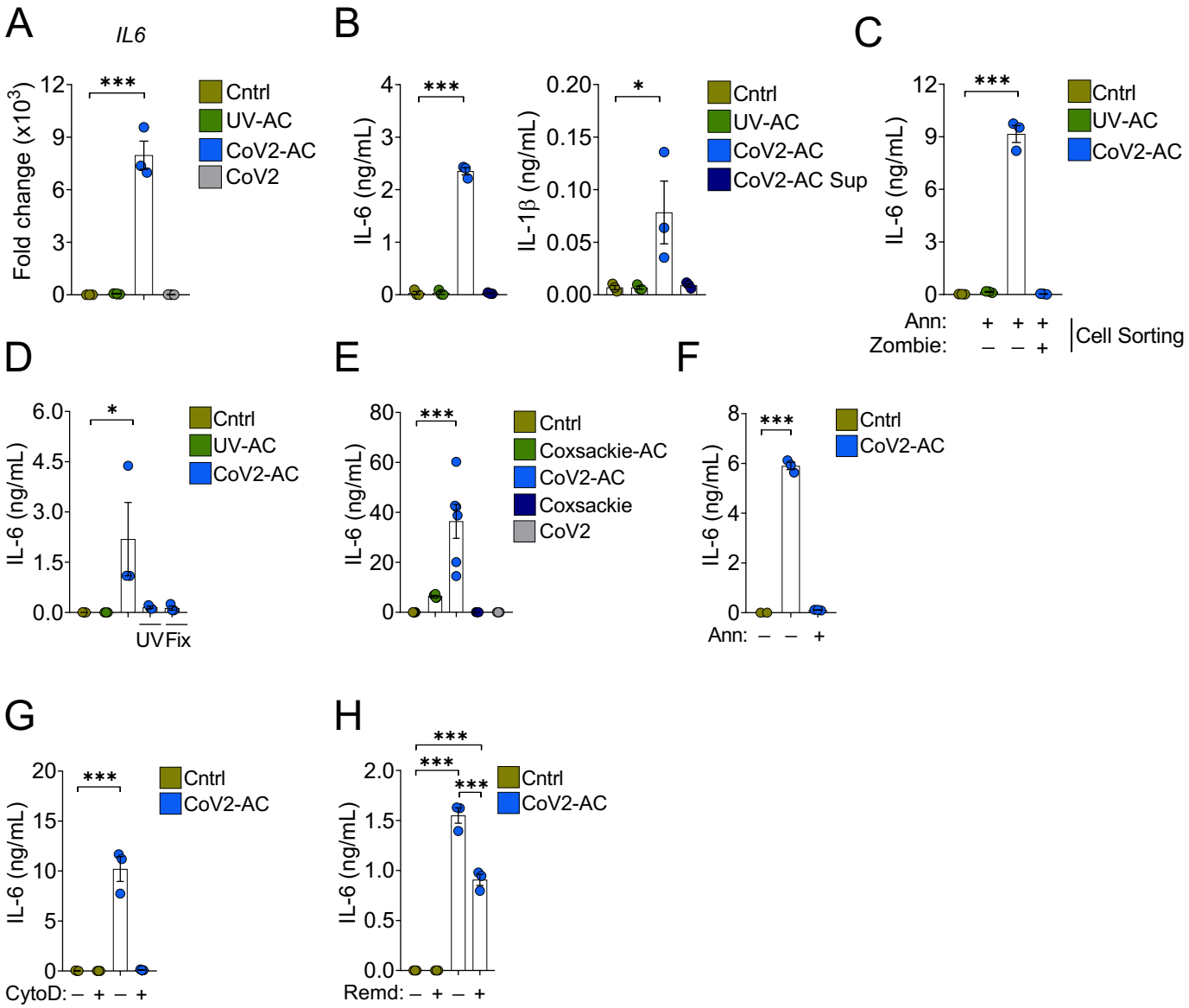

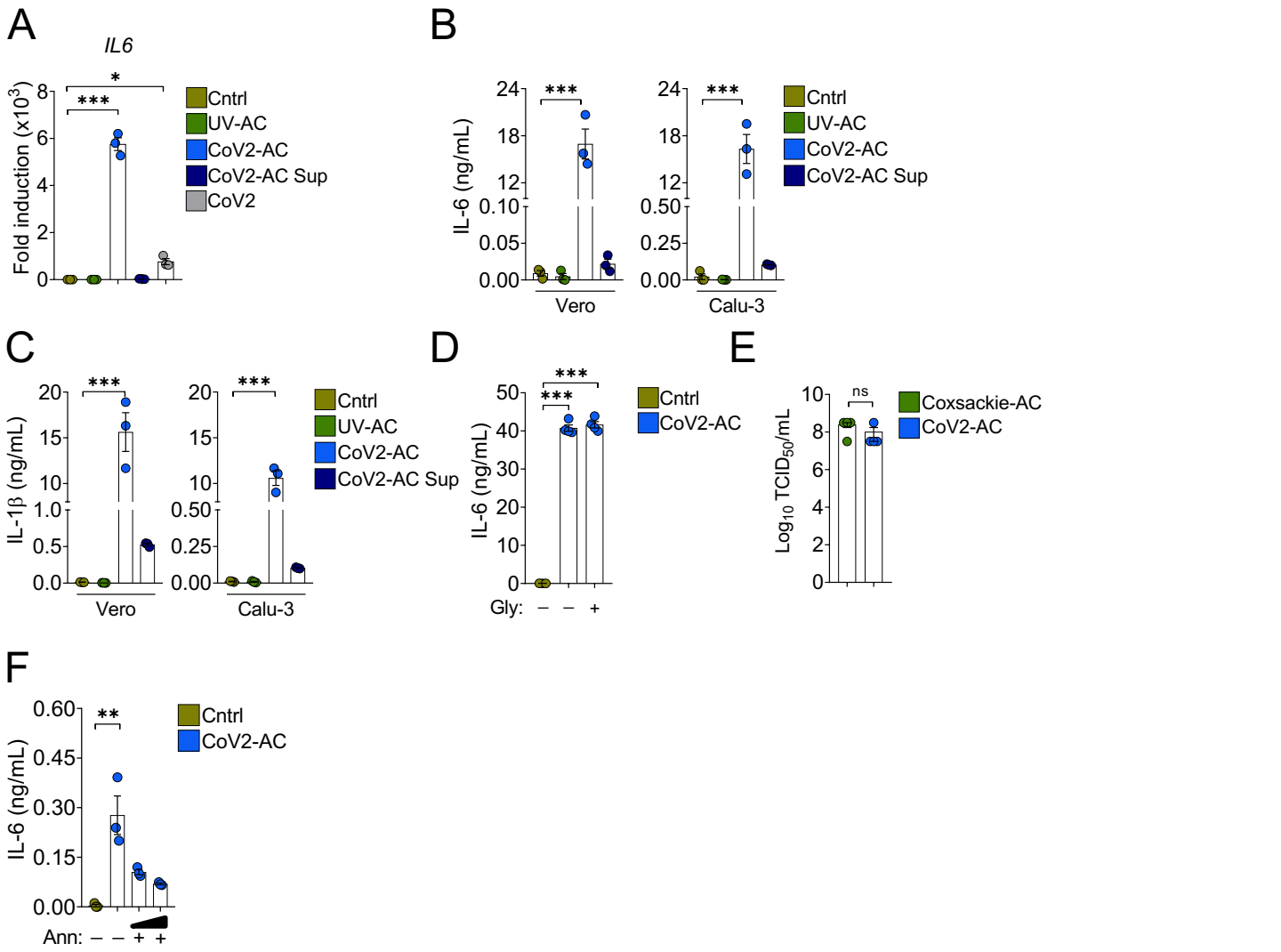

Figure 4

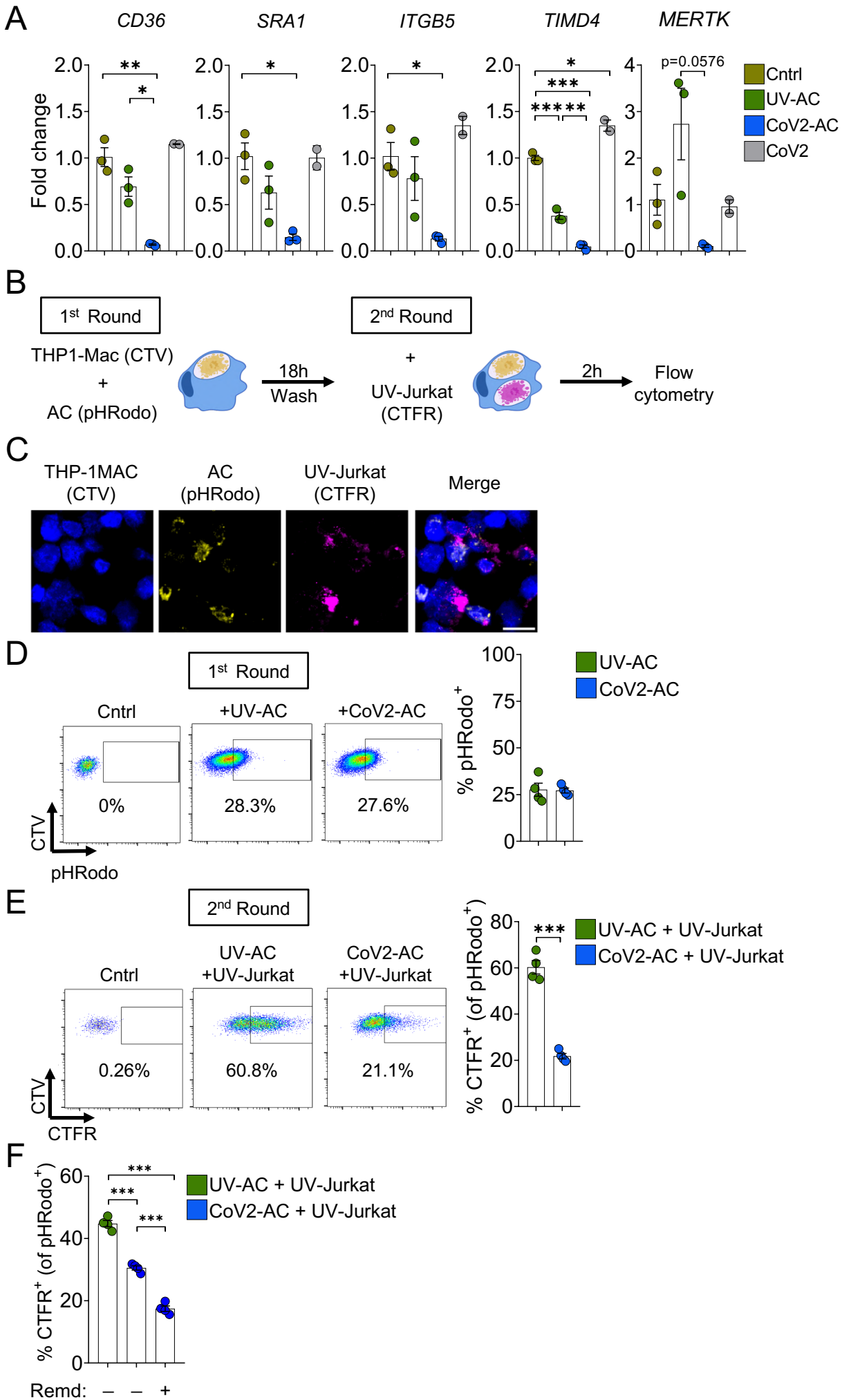

Figure 5

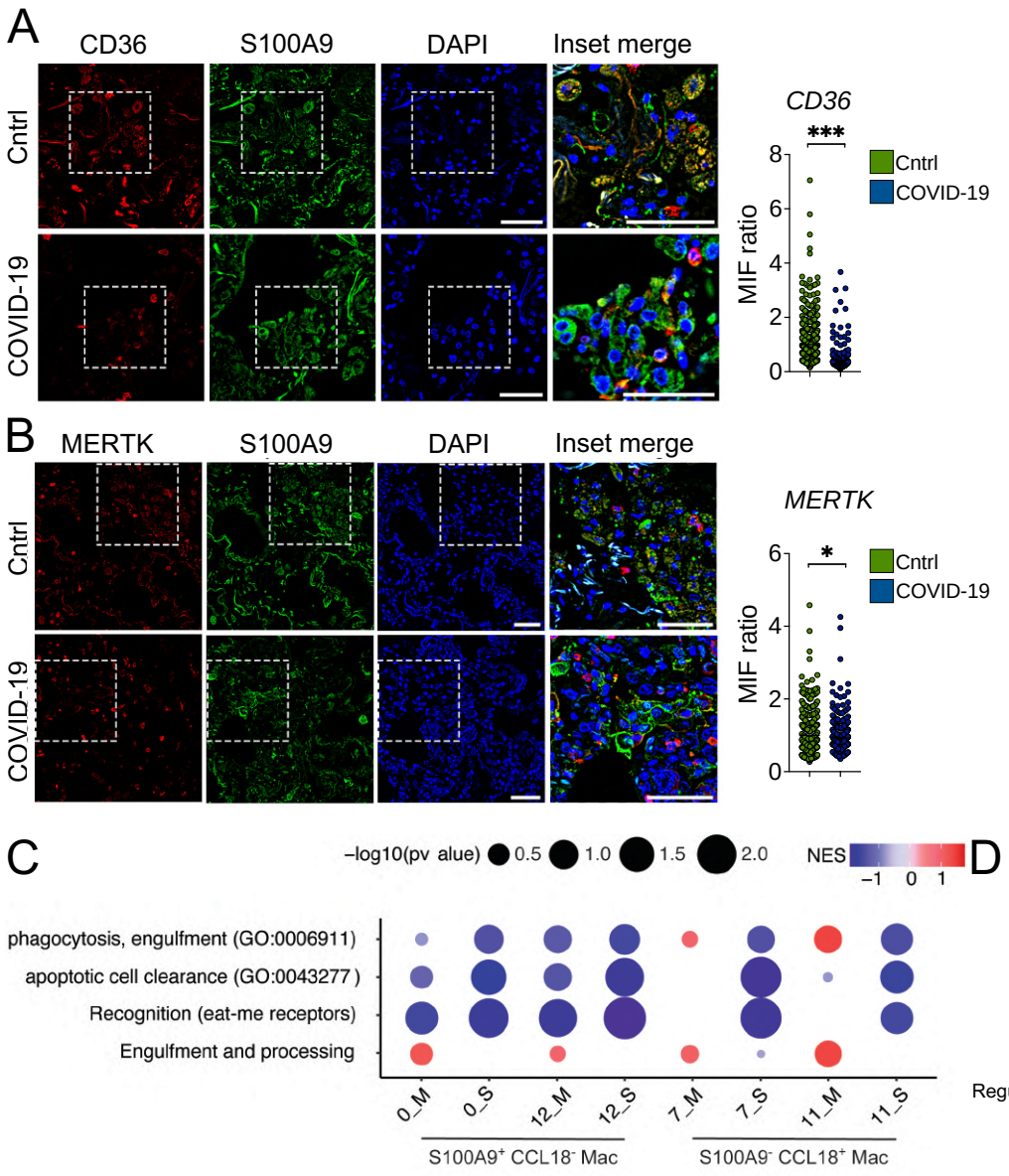

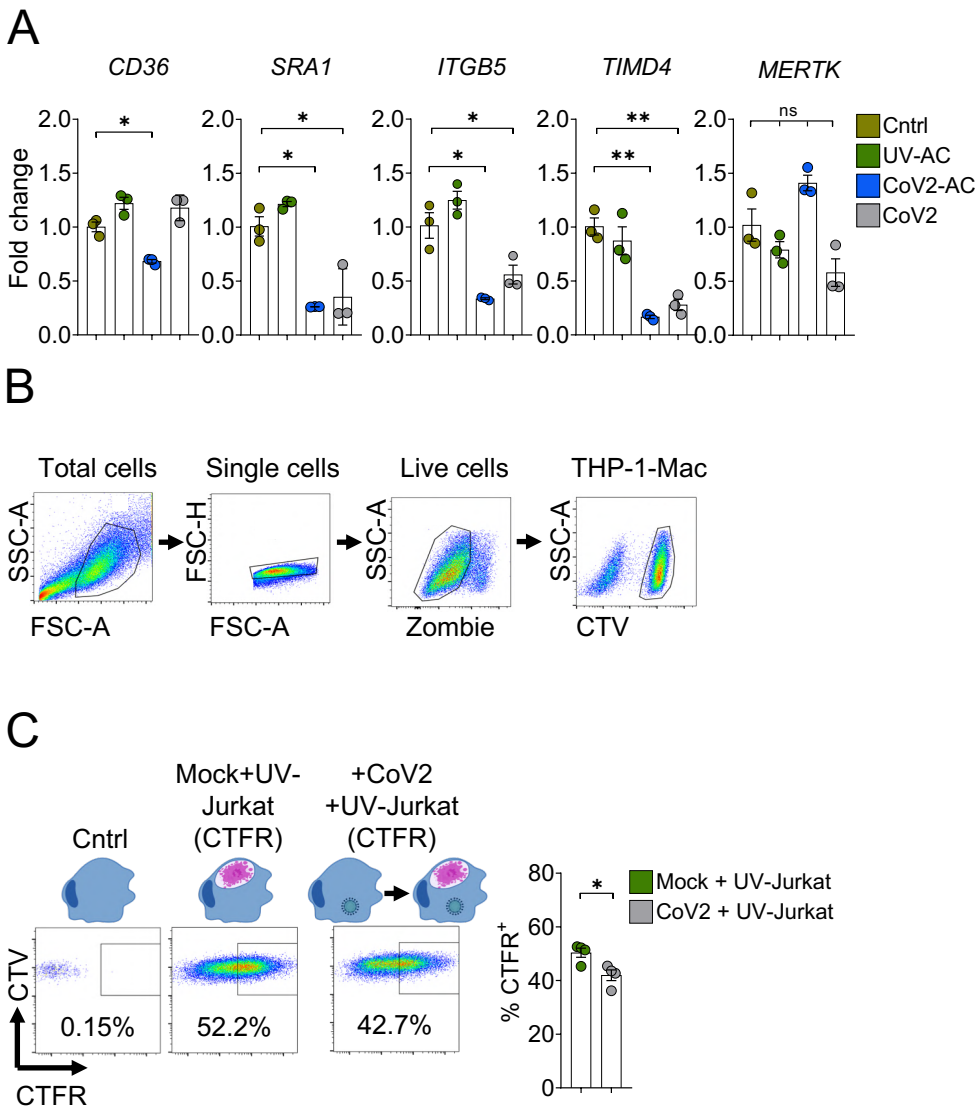

Supplementary File 1. Custom gene sets incorporating genes associated to efferocytic pathways and related to human diseases (Penberthy and Ravichandran, 2016; Boada-Romero et al., 2020) (related to Figure 4C).

Term	Gene				
Recognition (eat-me receptors)	GAS6	SCARB1	MARCO	MEGF10	STAB1
	MERTK	ITGB3	MFGE8	MSR1	STAB2
	ADGRB1	ITGAV	AXL	TIMD4	AGER
	LRP1	CD36	TYRO3	C1QA	SCARF1
Engulfment and processing	RAC2	RHOBTB1	DNM1L	ABCA1	ATG7
	RAC1	RHOG	ELMO1	RUBCN	ATG16L1
	RHOH	RAB14	SLC2A1	BECN1	GULP
	TREX1	TYROBP	SLC12A4	PIK3C3	
	RHOBTB2	DOCK1	DNASE2	ATG5	

Supplementary File 2 - COVID-19 patients medical characteristics

	Demographics	%
Number	4	
Age	73.5 ± 7.7	
Female		50
	Comorbidities	
Hypertension	2	50
Obesity	1	25
Diabetes	2	50
History of smoking	1	25
Heart disease	3	75
	Laboratorial findings	
ALT (U/L)*	620.25 ± 1106.36	
AST (U/L)**	1234 ± 2278.72	
CRP (mg/dL)***	14.37 ± 5.04	
D-Dimers (µg/mL)#	2.38 ± 1.45	
LDH (mmol/L)##	3.05 ± 1.85	
Urea (mg/dL)###	147.45 ± 35.68	
	Respiratory status	
Mechanical ventilation	3	75
Nasal-cannula oxygen	3	75
pO2	72.65 ± 13.53	
SatO2	90.2 ± 7.2	
	Disease severity	
Mild	0	0
Moderate	0	0
Severe	4	100
	Outcome	
Death	4	0

*ALT: Alanine Transaminase (normal range 10-49 U/L);

**AST: Aspartate Aminotransferase (normal value <32 U/L);

***CRP: C-reactive protein (normal value <1.0 mg/dL);

#D-dimers (normal value <0.5µg/mL);

##LDH: Lactate Dehydrogenase (normal range 120-246 U/L);

###Urea (normal range 19-49 mg/dL);